ELSEVIER

Advances in Water Resources 24 (2001) 531–550

Advances in Water Resources

www.elsevier.com/locate/advwatres

A Boltzmann-based mesoscopic model for contaminant transport in flow systems

J.Q. Deng [a,*], M.S. Ghidaoui [a], W.G. Gray [b], K. Xu [a]

[a] *Department of Civil Engineering, The Hong Kong University of Science and Technology, Kowloon, Hong Kong*
[b] *Department of Civil Engineering and Geological Sciences, University of Notre Dame, Notre Dame, IN, USA*

Abstract

The objective of this paper is to demonstrate the formulation of a numerical model for mass transport based on the Bhatnagar–Gross–Krook (BGK) Boltzmann equation. To this end, the classical chemical transport equation is derived as the zeroth moment of the BGK Boltzmann differential equation. The relationship between the mass transport equation and the BGK Boltzmann equation allows an alternative approach to numerical modeling of mass transport, wherein mass fluxes are formulated indirectly from the zeroth moment of a difference model for the BGK Boltzmann equation rather than directly from the transport equation. In particular, a second-order numerical solution for the transport equation based on the discrete BGK Boltzmann equation is developed. The numerical discretization of the first-order BGK Boltzmann differential equation is straightforward and leads to diffusion effects being accounted for algebraically rather than through a second-order Fickian term. The resultant model satisfies the entropy condition, thus preventing the emergence of non-physically realizable solutions including oscillations in the vicinity of the front. Integration of the BGK Boltzmann difference equation into the particle velocity space provides the mass fluxes from the control volume and thus the difference equation for mass concentration. The difference model is a local approximation and thus may be easily included in a parallel model or in accounting for complex geometry. Numerical tests for a range of advection–diffusion transport problems, including one- and two-dimensional pure advection transport and advection–diffusion transport show the accuracy of the proposed model in comparison to analytical solutions and solutions obtained by other schemes. © 2001 Published by Elsevier Science Ltd.

Keywords: Kinetic theory; Mesoscopic model; Advection–diffusion; Numerical model; Finite volume; Boltzmann equation

1. Introduction

Conventional numerical models are based on applying the method of characteristics, finite elements, or finite differences to solve macroscopic equations for a continuum based on conservation principles such as the advection–diffusion equation, shallow water equations, Euler equations and Navier–Stokes equations. Recently, the Boltzmann equation has been found to provide an alternative approach for the formulation of numerical models describing a wide range of fluid mechanics problems. The advent of Boltzmann-based schemes came about from the realization that, with the Chapman–Enskog expansion, fundamental conservation equations can be obtained as moments of the Bhatnagar–Gross–Krook (BGK) Boltzmann equation (see e.g., [7,20,29,32,33]). The relationship between the macroscopic conservation laws and the BGK Boltzmann equation prompted numerical modelers to formulate difference equations for the macroscopic variables as moments of a difference representation of the BGK Boltzmann equation.

The formulation of the BGK Boltzmann numerical technique herein consists of three components: (i) a check for consistency of the equations being solved; (ii) a discretization of the BGK Boltzmann equation in coordinate space; (iii) integration of the discrete equation over particle velocity space. The consistency check involves ensuring that the macroscopic equations that describe the process of interest can indeed be obtained as moments of the BGK Boltzmann equation through the introduction of appropriate relationships between the mesocopic and macroscopic variables. Macroscopic laws based on conservation principles, such as the Navier–Stokes equation, are obtained from moments of second-order approximation to the BGK Boltzmann equation, where the second-order error parameter is of

* Corresponding author.

0309-1708/01/$ - see front matter © 2001 Published by Elsevier Science Ltd.
PII: S0309-1708(00)00044-0

the order of the ratio of molecular to macroscopic length scales [29]. As this parameter is typically negligibly small, the approximation of the conservation equations is highly accurate. In the process of recovering macroscopic conservation for different applications, the relationship between mesoscopic and macroscopic variables and the number of moments required for a particular equation will depend on the application. However, the generic form of the underlying BGK Boltzmann equation does not change. For example, the BGK Boltzmann equation used to recover the two-dimensional Navier–Stokes equation is identical to that used to recover the shallow water equations or a two-dimensional mass or energy transport equation. The fact that problems which appear different at the macroscopic level are in fact, similar at the mesoscopic level is well illustrated by the following statement of Feynman (reported in Ref. [24, p. 4]):

> We have noticed in nature that the behavior of fluids depends very little on the nature of the individual particles in that fluid. For example, the flow of sand is very similar to the flow of water or the flow of ball bearings.

In the framework of the BGK Boltzmann method, the macroscale differential equations are not discretized and solved. Rather, the discretization step entails formulating a difference scheme for the BGK Boltzmann equation. Given that the generic form of the BGK Boltzmann equation from which momentum, mass, and energy transport equations are obtained, a BGK difference equation constructed for one application can be employed for other applications. For example, the difference form of the BGK Boltzmann equation used in the formulation of a numerical scheme for shock waves in gas dynamics [32,33] is identical to that used in the formulation of a numerical scheme in shallow waters [7]. This same discrete BGK Boltzmann equation is used in the present paper for the formulation of a numerical solution to the advection–diffusion equation.

The third formulation step involves integration of the difference form of the BGK Boltzmann equation in particle velocity space to obtain difference equations in terms of the macroscopic variables such as flow velocity, pressure and density. The integration step thus involves establishing a link between the particle distribution function and the macroscopic variables. The integration from mesoscopic to macroscopic variables is typically straightforward and requires the determination of moments of a Gaussian distribution. It is worth emphasizing that it is in the integration step, where the difference equations for macroscopic state variables emerge from the difference form of the BGK Boltzmann equation.

Examples where Boltzmann based models have been applied include shock waves in compressible flows (e.g., [3,20,32,33]), multicomponent and multiphase flows (e.g., [8,9,30]), flows in complex geometries (e.g., [1,23]), turbulent flows (e.g., [2,17]), low Mach number flows (e.g., [26]), heat transfer and reaction diffusion flows (e.g., [19,31]), and open channel flows (e.g., [4,7]). These applications revealed a number of advantages of Boltzmann based schemes. For instance, numerical models based on the collisional Boltzmann theory are found to satisfy the condition that entropy production in an isolated process cannot be negative. Thus they preclude the possibility of physically non-realizable solutions being obtained [7,33]. Boltzmann based schemes have been noted for the ease with which they can be extended to multi-dimensional cases and for their local character which makes them ideal for implementation in parallel computers [1,14]. Furthermore, Boltzmann based techniques have been found to be well suited for problems with complex geometry and boundary conditions [1,6,11,20]. Additionally, using a Boltzmann based scheme, [26] showed that incompressible flow solutions can be obtained in the limit as Mach number tends to zero. This observation allows the tedious and difficult solution of the Poisson's equation for the pressure field, required in traditional approaches to solve the incompressible flow equations, to be avoided. The fact that the Boltzmann equation has a simple form and that this equation is kinetic in nature makes the incorporation of additional physics straightforward [1,9]. The diffusion and viscous terms that appear as second derivative terms in macroscopic modeling are represented by a simple algebraic difference term in mesoscopic modeling. This eliminates the need for separate treatment of the advection and diffusion terms.

The objective of the current work is to explore the applicability of the BGK Boltzmann equation in the formulation of a numerical model for the advection and diffusion of a chemical contaminant. To this end, it is shown that the classical partial differential equation for mass transport is derivable from the zeroth moment of the BGK Boltzmann differential equation. Demonstration of this relationship allows one to then formulate the discrete Boltzmann equation and then integrate it to obtain a discrete equation in terms of concentrations of the chemical constituent. In particular, a second-order numerical solution for the integrated BGK Boltzmann equation, used by [32,33] for gas dynamics and [7], is adopted. This difference model satisfies the entropy condition, thus preventing the emergence of non-physically realizable solutions such as oscillations and overshoot in the vicinity of sharp concentration fronts. The resulting difference model depends on concentrations at the center and boundaries of the local computational cell. Interpolation approaches are introduced to relate these quantities over a discretization region. Numerical tests for a range of advection–diffusion transport problems in one- and two-dimensions are performed to provide a basis for the comparison of the attributes of

the Boltzmann-based model with the analytical solutions and solutions obtained by other schemes. Based on the accuracy and robustness of the solutions obtained, the possibility of using the BGK Boltzmann equation as an alternative approach to the numerical solution of mass transport is established.

In the Section 2, a discussion is provided to distinguish the present approach from existing ones and to motivate the usage and features of the BGK Boltzmann scheme. Then in the subsequent sections, the three steps to establishing the form of the BGK Boltzmann model for chemical transport will be performed. Finally, computed results for the test problems will be displayed.

2. Distinguishing features of the BGK Boltzmann approach

One of the persisting challenges in the numerical solution of conservation equations is the development of accurate algorithms for the simulation of advection-dominated processes and systems containing shocks. Two currently advocated approaches may be classified as flux difference splitting schemes (FDS) and flux vector splitting schemes (FVS). The general features of these methods will be indicated here to provide a context that motivates the BGK Boltzmann approach.

To provide a setting for this discussion, the following two-dimensional system of partial differential equations in Cartesian coordinates is considered:

$$\frac{\partial \mathbf{u}}{\partial t}+\frac{\partial \mathbf{r}}{\partial x}+\frac{\partial \mathbf{s}}{\partial y}=0, \tag{1}$$

where $\mathbf{u}$ is the vector of conserved variables $\mathbf{r}$ and $\mathbf{s}$ and are the total fluxes of $\mathbf{u}$ in the x- and y-coordinate directions, respectively. Each of the fluxes is a sum of an advective and a dispersive contribution such that

$$\mathbf{r}=\mathbf{r}_{\mathrm{a}}+\mathbf{r}_{\mathrm{d}} \tag{2a}$$

and

$$\mathbf{s}=\mathbf{s}_{\mathrm{a}}+\mathbf{s}_{\mathrm{d}}. \tag{2b}$$

Integration of Eq. (1) over a finite volume $[t^n,t^{n+1}]\times[x_{i-1/2},x_{i+1/2}]\times[y_{j-1/2},y_{j+1/2}]$ provides

$$\begin{aligned}\mathbf{U}_{i,j}^{n+1}-\mathbf{U}_{i,j}^{n}&+\frac{1}{\Delta x\Delta y}\int_{t^n}^{t^{n+1}}\int_{y_{j-1/2}}^{y_{j+1/2}}(\mathbf{r}_{\mathrm{a}_{i+1/2}}-\mathbf{r}_{\mathrm{a}_{i-1/2}})\,\mathrm{d}y\,\mathrm{d}t\\&+\frac{1}{\Delta x\Delta y}\int_{t^n}^{t^{n+1}}\int_{y_{j-1/2}}^{y_{j+1/2}}(\mathbf{r}_{\mathrm{d}_{i+1/2}}-\mathbf{r}_{\mathrm{d}_{i-1/2}})\,\mathrm{d}y\,\mathrm{d}t\\&+\frac{1}{\Delta x\Delta y}\int_{t^n}^{t^{n+1}}\int_{x_{i-1/2}}^{x_{i+1/2}}(\mathbf{s}_{\mathrm{a}_{j+1/2}}-\mathbf{s}_{\mathrm{a}_{j-1/2}})\,\mathrm{d}x\,\mathrm{d}t\\&+\frac{1}{\Delta x\Delta y}\int_{t^n}^{t^{n+1}}\int_{x_{i-1/2}}^{x_{i+1/2}}(\mathbf{s}_{\mathrm{d}_{j+1/2}}-\mathbf{s}_{\mathrm{d}_{j-1/2}})\,\mathrm{d}x\,\mathrm{d}t=0,\end{aligned} \tag{3}$$

where $\mathbf{U}_{i,j}^{n}$ is the average value of $\mathbf{u}$ over the spatial coordinates of the volume at time t^n. Solution of Eq. (3) to obtain an approximate value $\mathbf{U}_{i,j}^{n+1}$ requires that procedures be employed to approximate the integrals in Eq. (3). Several of these methods will now be discussed.

FDS schemes (e.g., [5,18,21,22]) provide approximations for the integrals of the advective fluxes in Eq. (3) based on the approximate solution of the Riemann problem. It is quite instructive to review how the Riemann problem, on which FDS schemes are based, is obtained. The FDS scheme splits the fluxes in the differential equation into the advective and dispersive parts and deals with these separately. First, the advective problem is solved by breaking it into two one-dimensional problems

$$\frac{\partial \mathbf{u}}{\partial t}+\frac{\partial \mathbf{r}_{\mathrm{a}}}{\partial x}=0 \quad \text{and} \quad \frac{\partial \mathbf{u}}{\partial t}+\frac{\partial \mathbf{s}_{\mathrm{a}}}{\partial y}=0 \tag{4}$$

that may also be expressed as

$$\frac{\partial \mathbf{u}}{\partial t}+\mathbf{A}\cdot\frac{\partial \mathbf{u}}{\partial x}=0 \quad \text{and} \quad \frac{\partial \mathbf{u}}{\partial t}+\mathbf{B}\cdot\frac{\partial \mathbf{u}}{\partial y}=0, \tag{5}$$

where $\mathbf{A}$ and $\mathbf{B}$ are Jacobian matrices with

$$\mathbf{A}=\frac{\partial \mathbf{r}_{\mathrm{a}}}{\partial \mathbf{u}} \quad \text{and} \quad \mathbf{B}=\frac{\partial \mathbf{s}_{\mathrm{a}}}{\partial \mathbf{u}}. \tag{6}$$

The Jacobian matrices are generally non-linear. FDS schemes employ linearized approximations to these matrices, and the main differences among various implementations of FDS are related to the approximation used. Here, assume that some linearization method is employed that converts $\mathbf{A}$ and $\mathbf{B}$ to $\bar{\mathbf{A}}$ and $\bar{\mathbf{B}}$, respectively, where the overbar indicates a linearization. Thus the split equations become

$$\frac{\partial \mathbf{u}}{\partial t}+\bar{\mathbf{A}}\cdot\frac{\partial \mathbf{u}}{\partial x}=0 \quad \text{and} \quad \frac{\partial \mathbf{u}}{\partial t}+\bar{\mathbf{B}}\cdot\frac{\partial \mathbf{u}}{\partial y}=0. \tag{7}$$

From the known information at t^n, these equations are solved by characteristic decomposition for values of $\mathbf{u}$ at the interfaces between the discrete volumes. These solutions for $\mathbf{u}$ are then employed to obtain the FDS advective fluxes and dispersive fluxes for use in Eq. (3). Thus, the FDS scheme consists of splitting of the conservation equations in space; computation of FDS fluxes with dispersion neglected using a linearized advective operator from piecewise constant initial conditions using the method of characteristics; introduction of the FDS fluxes and a dispersion flux (computed, for example, using a central difference technique) into the model Eq. (3) for solution of $\mathbf{U}_{i,j}^{n+1}$.

FVS schemes (e.g., [25,28]) belong to the same class as FDS schemes in the sense that they are both upwinding techniques. As with the FDS method, the FVS splits Eq. (1) to obtain Eq. (4). However, FVS methods employ a different procedure for approximating the advective fluxes. A central requirement for FVS is that

the fluxes, $\mathbf{r}_a$ and $\mathbf{s}_a$ must be homogeneous [10] such that, for an arbitrary parameter λ

$$\mathbf{r}_a(\lambda\mathbf{u}) = \lambda\mathbf{r}_a(\mathbf{u}) \quad \text{and} \quad \mathbf{s}_a(\lambda\mathbf{u}) = \lambda\mathbf{s}_a(\mathbf{u}). \tag{8}$$

Differentiation of these relations with respect to λ yields

$$\frac{\partial[\mathbf{r}_a(\lambda\mathbf{u})]}{\partial(\lambda\mathbf{u})} \cdot \frac{\mathrm{d}(\lambda\mathbf{u})}{\mathrm{d}\lambda} = \frac{\partial[\mathbf{r}_a(\lambda\mathbf{u})]}{\partial(\lambda\mathbf{u})} \cdot \mathbf{u} = \mathbf{r}_a(\mathbf{u}) \tag{9a}$$

and

$$\frac{\partial[\mathbf{s}_a(\lambda\mathbf{u})]}{\partial(\lambda\mathbf{u})} \cdot \frac{\mathrm{d}(\lambda\mathbf{u})}{\mathrm{d}\lambda} = \frac{\partial[\mathbf{s}_a(\lambda\mathbf{u})]}{\partial(\lambda\mathbf{u})} \cdot \mathbf{u} = \mathbf{s}_a(\mathbf{u}). \tag{9b}$$

Then, if these equations are evaluated for the case of $\lambda = 1$ and Eq. (6) are imposed, one obtains

$$\frac{\partial[\mathbf{r}_a(\mathbf{u})]}{\partial(\mathbf{u})} \cdot \mathbf{u} = \mathbf{A} \cdot \mathbf{u} = \mathbf{r}_a(\mathbf{u}) \quad \text{and}$$
$$\frac{\partial[\mathbf{s}_a(\mathbf{u})]}{\partial(\mathbf{u})} \cdot \mathbf{u} = \mathbf{B} \cdot \mathbf{u} = \mathbf{s}_a(\mathbf{u}). \tag{10}$$

FVS schemes decompose the Jacobian matrices according to

$$\mathbf{A} = \mathbf{A}^+ + \mathbf{A}^- \quad \text{and} \quad \mathbf{B} = \mathbf{B}^+ + \mathbf{B}^-, \tag{11}$$

where $\mathbf{A}^+$ and $\mathbf{B}^+$ are associated with positive characteristics $\mathbf{A}^-$ and $\mathbf{B}^-$ and are associated with negative characteristics. Thus, the fluxes in Eq. (10) decompose as

$$\mathbf{A}^+ \cdot \mathbf{u} + \mathbf{A}^- \cdot \mathbf{u} = \mathbf{r}_a^+ + \mathbf{r}_a^- = \mathbf{r}_a \quad \text{and}$$
$$\mathbf{B}^+ \cdot \mathbf{u} + \mathbf{B}^- \cdot \mathbf{u} = \mathbf{s}_a^+ + \mathbf{s}_a^- = \mathbf{s}_a. \tag{12}$$

Note that if the fluxes were not homogeneous, the decomposition of $\mathbf{A}$ and $\mathbf{B}$ is still mathematically possible, but the parts would not be associated with the physical characteristic curves. Substitution of Eq. (12) into Eq. (4) yields

$$\frac{\partial \mathbf{u}}{\partial t} + \frac{\partial \mathbf{r}_a^+}{\partial x} + \frac{\partial \mathbf{r}_a^-}{\partial x} = 0 \quad \text{and} \quad \frac{\partial \mathbf{u}}{\partial t} + \frac{\partial \mathbf{s}_a^+}{\partial y} + \frac{\partial \mathbf{s}_a^-}{\partial y} = 0. \tag{13}$$

The solutions to these equations are based on approximating the gradients of the fluxes using upstream or downstream values of the gradient of the flux interpolated from the conditions at time t^n. Then the relation given in Eq. (10) provides the fluxes at the cell interfaces that are employed in Eq. (3). As with the FDS method, central difference approximations are used to estimate the dispersive fluxes. Thus, the first step of FVS consists of splitting the conservation equations in space that neglect the dispersive flux with the advective operator expressed in a homogeneous form. Then the characteristic decomposition is performed to resolve the positive and negative characteristics for use in the solution.

The major difference between the FDS and FVS schemes is that FDS schemes include the interaction between positive and negative waves at the cell interfaces but FVS schemes allow the positive and negative waves to cross the cell interface but without interacting. Nevertheless, a proper choice of the interpolative scheme for the construction of initial conditions for FVS schemes and other artificially added terms have been found to make FDS and FVS schemes identical.

While FVS and FDS schemes require a directional split and a split of the physics of advection and diffusion to estimate advective fluxes based on wave direction, BGK schemes do not require these splits and do not resolve waves. Fundamentally, the FVS and FDS approaches are based on the macroscopic behavior of the flow while the BGK Boltzmann is based on the mesoscopic behavior of the flow. To explain, the physics of advection and diffusion are a manifestation of adopting the continuum approach. In fact, macroscopic advection is nothing but the mean motion of the random velocity of atoms that make up the continuum; and macroscopic dispersion is due to the fluctuations around this mean. The Boltzmann theory gives an equation that governs the probability distribution of molecular speeds.

Since only molecular motion is monitored at the mesoscopic level, the BGK Boltzmann approach simply states that: the total advective and dispersive mass fluxes entering a finite volume across the boundaries of the volume are simply equal to the net mass of particles that enter the volume. The Boltzmann distribution of particle speeds, f, at a particular location defines how the mass of particles is distributed among the speeds. Thus, fluxes are split between particles that move in the positive and negative coordinate directions. For emphasis, note that in the BGK scheme, as compared to the FDS and FVS schemes, all splitting is done on a scalar function, f, rather than on a vector flux function and the splitting is accomplished simply without linearization of matrix decomposition.

The details of how the function f is obtained and of the implementation of the BGK Boltzmann procedure are explored in the subsequent sections of this manuscript. However, based on the preliminary discussion here, it is possible to identify the following advantageous features of the BGK approach:

- The diffusion and viscous terms that appear as second derivative terms in macroscopic modeling are represented by a simple algebraic difference term in mesoscopic modeling. This eliminates the need for separate treatment of the advection and diffusion terms. FVS and FDS schemes can only model advective terms. The BGK automatically gives the total flux.
- Boltzmann-based schemes have been noted for the ease by which they can be extended to multi-dimensional cases and for their local character that makes them ideal for implementation in parallel computers [1,14]. This simplicity arises because the construction of BGK fluxes is based on a scalar function while the FVS and FDS procedures are based on vector quantities and require a directional splitting in treating multi-dimensional problems.

- Boltzmann-based techniques have been found to be well suited for problems with complex geometry and boundary conditions [1,6,11,20]. The advantage here arises from the fact that the BGK scheme makes use of particle velocities and not characteristic curves in solving a single scalar equation that can be easily written in various coordinate systems.
- Using a Boltzmann-based scheme, [26] have showed that incompressible flow solutions can be obtained in the limit as the Mach number tends to zero. Thus, the tedious and difficult solution of the Poisson's equation that describes the pressure field in incompressible flow is avoided. FVS and FDS schemes employ characteristic curves. As a flow tends toward incompressible, the characteristic propagation speeds become infinite and these schemes fail. On the other hand, BGK schemes are based on particle speeds and not characteristic curves and thus are not impacted at the incompressible limit.
- Numerical models based on the collisional Boltzmann theory have been shown to satisfy the entropy condition; thus, precluding the emergence of physically non-realizable solutions [7,33]. The moments of the Boltzmann equations not only provide the macroscale conservation laws of mass, momentum and energy but also the entropy equation. Hence, the solution that is based on Boltzmann equation implicitly satisfies the entropy equation. However, FVS and FDS schemes only satisfy one-dimensional advection equations in different directions. The directional splitting alone can produce solutions that do not satisfy the entropy condition. The paper by Quirk [34] discusses the failures of FDS schemes.

Despite these attractive features, the BGK Boltzmann scheme is not always superior to other procedures. The application of the BGK schemes rests on the premise that the model to be solved can be recovered from the Boltzmann equation. If this cannot be accomplished, the BGK scheme cannot be adopted.

In the subsequent sections, the formulation of the BGK-based flux of mass transport is based on the full Boltzmann equation. However, it is possible to simplify the formulation by directional splitting of the Boltzmann equation. However, [13] have showed that the BGK flux obtained from directional splitting of the Boltzmann equation is a non-linear amalgamation of the Lax–Wendroff scheme and FVS. In addition, they showed that the BGK scheme approaches the Lax–Wendroff scheme as the molecular collision time tends to zero; and it approaches the FVS scheme as the collision time tends to infinity. This implies that FVS schemes are highly diffusive.

The essence of the preceding discussion is that the BGK schemes and lattice Boltzmann schemes have their roots in the mesoscale molecular dynamics of the flow, while classical schemes have their roots in macroscopic behavior. Building on these ideas it is possible to develop conservation equations of mass, momentum, and energy as moments of the Boltzmann equation. The objective here is less comprehensive and more illustrative as we wish only to provide the three-step derivation appropriate for species transport and then demonstrate a suite of solutions to this equation.

3. Consistency of the mesoscopic model with the macroscale transport model

The two-dimensional BGK Boltzmann equation is written as follows [7,12,33]:

$$\frac{\partial f}{\partial t}+c_x\frac{\partial f}{\partial x}+c_y\frac{\partial f}{\partial y}+\frac{F_x}{m}\frac{\partial f}{\partial c_x}+\frac{F_y}{m}\frac{\partial f}{\partial c_y}=\frac{q-f}{\tau} \tag{14a}$$

or, in vector notation as

$$\frac{\partial f}{\partial t}+\mathbf{c}\cdot\nabla f+\frac{1}{m}\mathbf{F}\cdot\frac{\partial f}{\partial \mathbf{c}}=\frac{q-f}{\tau}, \tag{14b}$$

where subscripts x and y refer to vector components in the **x**-coordinate space, **c** the velocity vector of a particle in the two-dimensional space; t the time, ∇ the two-dimensional nabla operator, m the mass of a particle, **F** the net external force acting on the particles in the coordinate directions, τ the collision time and will be discussed subsequently, $f(\mathbf{x},\mathbf{c},t)$ the non-equilibrium distribution function of particles that comprise the species of interest, and $q(\mathbf{x},\mathbf{c},t)$ the equilibrium distribution function of particles that can be determined by maximizing the entropy function [7]. Note that the right-hand side of the preceding equation is a measure of disequilibrium of the distribution function and that f for the species of interest is different from f for the entire fluid phase.Eq. (14b) may be written in terms of the total derivative of the distribution function f as

$$\frac{\mathrm{d}f}{\mathrm{d}t}=\frac{q-f}{\tau}, \tag{15a}$$

when

$$\frac{\mathrm{d}\mathbf{x}}{\mathrm{d}t}=\mathbf{c} \tag{15b}$$

and

$$\frac{\mathrm{d}\mathbf{c}}{\mathrm{d}t}=\frac{\mathbf{F}}{m}. \tag{15c}$$

The equilibrium particle distribution function for the chemical constituent of interest is given by the following Gaussian distribution [7]:

$$q(\mathbf{x},\mathbf{c},t)=C\frac{\lambda}{\pi}\exp[-\lambda|\mathbf{c}-\mathbf{v}|^2], \tag{16}$$

where **v** is the macroscale advective velocity vector of the fluid, C is the contaminant concentration, and λ is a measure of the distribution of particle velocities.

The macroscopic concentration C is related to the mesoscopic variable f as follows [32]:

$$C = \int_{-\infty}^{\infty}\int_{-\infty}^{\infty} f \,\mathrm{d}c_x \,\mathrm{d}c_y \tag{17}$$

and the integral of the first moment of f is the flux function of the chemical species, $\mathbf{N}$, where

$$\mathbf{N} = \int_{-\infty}^{\infty}\int_{-\infty}^{\infty} \mathbf{c} f \,\mathrm{d}c_x \,\mathrm{d}c_y. \tag{18}$$

If a fluctuation particle velocity for the chemical constituent of interest is defined as $\mathbf{c}' = \mathbf{c} - \mathbf{v}$, where $\mathbf{v}$ is the flow velocity and $\mathbf{c}$ is the particle velocity of the chemical species, then Eq. (18) may be written

$$\mathbf{N} = \mathbf{v}C + \int_{-\infty}^{\infty}\int_{-\infty}^{\infty} \mathbf{c}'(f-q) \,\mathrm{d}c_x \,\mathrm{d}c_y, \tag{19}$$

where the first term on the right-hand side is the advective flux. The integral term accounts for dispersion of the chemical species under study, and the integrand is a product of the deviation of species particle velocities from the mean flow velocity and the deviation of the distribution function of the species from its equilibrium form. The fact that mass is collision invariant (i.e., no chemical reactions are being considered) provides the restriction that

$$0 = \int_{-\infty}^{\infty}\int_{-\infty}^{\infty} \frac{q-f}{\tau} \,\mathrm{d}c_x \,\mathrm{d}c_y. \tag{20}$$

To obtain the mass transport equation, it is necessary to integrate Eq. (14b) over the particle velocities to obtain

$$\int_{-\infty}^{\infty}\int_{-\infty}^{\infty} \frac{\partial f}{\partial t} \,\mathrm{d}c_x \,\mathrm{d}c_y + \int_{-\infty}^{\infty}\int_{-\infty}^{\infty} \mathbf{c}\cdot\nabla f \,\mathrm{d}c_x \,\mathrm{d}c_y + \int_{-\infty}^{\infty}\int_{-\infty}^{\infty} \frac{1}{m}\mathbf{F}\cdot\frac{\partial f}{\partial \mathbf{c}} \,\mathrm{d}c_x \,\mathrm{d}c_y = \int_{-\infty}^{\infty}\int_{-\infty}^{\infty} \frac{q-f}{\tau} \,\mathrm{d}c_x \,\mathrm{d}c_y. \tag{21}$$

From Eq. (20), the right-hand side of Eq. (21) is zero. Also, $\mathbf{F}/m$ is an external force term that is independent of the particle velocity distribution. Thus, it may be moved outside the integral. Then integration of the third term shows that this integral is zero. The integrands of the first two integrals may be added together. Also, the order of integration and differentiation may be rearranged in Eq. (21) to obtain

$$\frac{\partial}{\partial t}\int_{-\infty}^{\infty}\int_{-\infty}^{\infty} f \,\mathrm{d}c_x \,\mathrm{d}c_y + \nabla\cdot\int_{-\infty}^{\infty}\int_{-\infty}^{\infty} \mathbf{c} f \,\mathrm{d}c_x \,\mathrm{d}c_y = 0 \tag{22}$$

or, after making use of Eqs. (17) and (18)

$$\frac{\partial C}{\partial t} + \nabla\cdot\mathbf{N} = 0. \tag{23}$$

Note that under conditions of an equilibrium distribution of particle velocities (i.e. when $f = q$), the flux term will be solely advective such that $\mathbf{N} = C\mathbf{v}$. However, when $f \neq q$, the flux term accounts for both advection and diffusion; but it is not obvious how the flux should be divided between these two processes. Since the form of f is not available precisely, discretization of the Boltzmann equation written in terms of f will be more difficult to relate to a macroscale discrete equation than a discretization of an approximate Boltzmann equation written in terms of the known equilibrium distribution function q. Therefore, it will be useful to express f via an expansion in terms of q and its derivatives. From Eq. (15a), f may be expressed as

$$f = q - \tau\frac{\mathrm{d}f}{\mathrm{d}t}. \tag{24}$$

Then substitution of this expression for f into the time derivative yields

$$f = q - \tau\left[\frac{\mathrm{d}q}{\mathrm{d}t} - \frac{\mathrm{d}}{\mathrm{d}t}\left(\tau\frac{\mathrm{d}f}{\mathrm{d}t}\right)\right]. \tag{25}$$

Note that τ is of the time scale of a particle collision, whereas t is at the macroscopic time scale, a scale at which f changes significantly. Therefore, it is convenient to write $\tau = \epsilon\hat{\tau}$, where ϵ is a small dimensionless constant of the order of the molecular collision time divided by the macroscopic time scale and $\hat{\tau}$ is of the same order as the macroscopic time scale. Thus, Eq. (25) becomes

$$f = q - \epsilon\hat{\tau}\left[\frac{\mathrm{d}q}{\mathrm{d}t} - \epsilon\frac{\mathrm{d}}{\mathrm{d}t}\left(\hat{\tau}\frac{\mathrm{d}f}{\mathrm{d}t}\right)\right]. \tag{26}$$

Further substitution of f may be employed to extend this expression to include higher derivatives of q and a final term involving a derivative of f. The form obtained may be truncated to read

$$f = q - \epsilon\hat{\tau}\frac{\mathrm{d}q}{\mathrm{d}t} + \epsilon^2\hat{\tau}\frac{\mathrm{d}}{\mathrm{d}t}\left(\hat{\tau}\frac{\mathrm{d}q}{\mathrm{d}t}\right) + \mathcal{O}(\epsilon^3). \tag{27}$$

Now substitution of this equation into Eq. (22) provides the expression

$$\frac{\partial}{\partial t}\int_{-\infty}^{\infty}\int_{-\infty}^{\infty} q \,\mathrm{d}c_x \,\mathrm{d}c_y - \frac{\partial}{\partial t}\int_{-\infty}^{\infty}\int_{-\infty}^{\infty} \epsilon\hat{\tau}\frac{\mathrm{d}q}{\mathrm{d}t} \,\mathrm{d}c_x \,\mathrm{d}c_y + \nabla\cdot\int_{-\infty}^{\infty}\int_{-\infty}^{\infty} \mathbf{c} q \,\mathrm{d}c_x \,\mathrm{d}c_y - \nabla\cdot\int_{-\infty}^{\infty}\int_{-\infty}^{\infty} \mathbf{c}\epsilon\hat{\tau}\frac{\mathrm{d}q}{\mathrm{d}t} \,\mathrm{d}c_x \,\mathrm{d}c_y + \mathcal{O}(\epsilon^2) = 0. \tag{28}$$

Each of the integrals in this equation may be evaluated as follows:

$$\frac{\partial}{\partial t}\int_{-\infty}^{\infty}\int_{-\infty}^{\infty} q \,\mathrm{d}c_x \,\mathrm{d}c_y = \frac{\partial C}{\partial t}, \tag{29a}$$

$$\frac{\partial}{\partial t}\int_{-\infty}^{\infty}\int_{-\infty}^{\infty} \epsilon\hat{\tau}\frac{\mathrm{d}q}{\mathrm{d}t} \,\mathrm{d}c_x \,\mathrm{d}c_y = \frac{\partial}{\partial t}\left\{\epsilon\hat{\tau}\left[\frac{\partial C}{\partial t} + \nabla\cdot(C\mathbf{v})\right]\right\}, \tag{29b}$$

$$\nabla\cdot\int_{-\infty}^{\infty}\int_{-\infty}^{\infty} \mathbf{c} q \,\mathrm{d}c_x \,\mathrm{d}c_y = \nabla\cdot(C\mathbf{v}), \tag{29c}$$

$$\nabla \cdot \int_{-\infty}^{\infty}\int_{-\infty}^{\infty} \mathbf{c}\epsilon\hat{\tau}\frac{\mathrm{d}q}{\mathrm{d}t}\,\mathrm{d}c_x\,\mathrm{d}c_y = \nabla \cdot \left\{\epsilon\hat{\tau}\left[\frac{\partial}{\partial t}(C\mathbf{v}) + \nabla \cdot \left[C\left(\mathbf{v}\mathbf{v} + \frac{1}{2\lambda}\mathbf{I}\right)\right]\right]\right\}. \quad (29d)$$

Then reconstitution of Eq. (28) yields

$$\frac{\partial C}{\partial t} + \nabla \cdot (C\mathbf{v}) - \frac{\partial}{\partial t}\left\{\epsilon\hat{\tau}\left[\frac{\partial C}{\partial t} + \nabla \cdot (C\mathbf{v})\right]\right\} - \nabla \cdot \left\{\epsilon\hat{\tau}\left[\frac{\partial}{\partial t}(C\mathbf{v}) + \nabla \cdot \left[C\left(\mathbf{v}\mathbf{v} + \frac{1}{2\lambda}\mathbf{I}\right)\right]\right]\right\} + \mathcal{O}(\epsilon^2) = 0. \quad (30)$$

Now to make the manipulations to follow more transparency, define a grouping of terms, M, such that

$$M = \frac{\partial C}{\partial t} + \nabla \cdot (C\mathbf{v}). \quad (31)$$

Then Eq. (30) may be directly reorganized to

$$M - \frac{\partial}{\partial t}[\epsilon\hat{\tau}M] - \nabla \cdot \left\{\epsilon\hat{\tau}C\left[\frac{\partial \mathbf{v}}{\partial t} + \mathbf{v} \cdot \nabla\mathbf{v} + \nabla\left(\frac{1}{2\lambda}\right)\right] + \epsilon\hat{\tau}\mathbf{v}M + \frac{\epsilon\hat{\tau}}{2\lambda}\nabla C\right\} + \mathcal{O}(\epsilon^2) = 0. \quad (32)$$

Thus, it can be seen that M is of $\mathcal{O}(\epsilon)$ so that any term containing ϵM is of $\mathcal{O}(\epsilon^2)$ and can be lumped in with the error term so that Eq. (32) becomes

$$M - \nabla \cdot \left\{\epsilon\hat{\tau}C\left[\frac{\partial \mathbf{v}}{\partial t} + \mathbf{v} \cdot \nabla\mathbf{v} + \nabla\left(\frac{1}{2\lambda}\right)\right] + \frac{\epsilon\hat{\tau}}{2\lambda}\nabla C\right\} + \mathcal{O}(\epsilon^2) = 0. \quad (33)$$

It can be shown (e.g., in Ref. [7], for shallow water flow; in Ref. [29], for the Navier–Stokes equation), that the term in square brackets is the momentum equation with error $\mathcal{O}(\epsilon)$, where the pressure divided by density can be identified as $1/(2\lambda)$ with units of L^2/T^2. Since this momentum expression is multiplied by ϵ, it is of order $\mathcal{O}(\epsilon^2)$ and may also be lumped with the error term leaving

$$M - \nabla \cdot \left[\frac{\epsilon\hat{\tau}}{2\lambda}\nabla C\right] + \mathcal{O}(\epsilon^2) = 0 \quad (34)$$

or, after reinstating the expression for M

$$\frac{\partial C}{\partial t} + \nabla \cdot (C\mathbf{v}) - \nabla \cdot \left[\frac{\epsilon\hat{\tau}}{2\lambda}\nabla C\right] = \mathcal{O}(\epsilon^2). \quad (35)$$

Thus, if a diffusion coefficient D is defined with units of L^2/T

$$D = \frac{\epsilon\hat{\tau}}{2\lambda}. \quad (36)$$

Eq. (35) represents a second-order approximation to the classical advection–diffusion equation. Recall that since ϵ is the ratio of the molecular time scale to the macroscopic time scale, the error is negligibly small. If ϵ is large (say of order 1), then the Boltzmann based scalar transport equation departs from the classical scalar transport equation. Therefore, it is tempting to conclude that the Boltzmann based model is incorrect in this case and that one needs to return to the classical scalar transport equation for modeling purposes. However, ϵ of order 1 means that the molecular and macroscopic length scales are of similar magnitude making the continuum hypotheses and thus the classical transport equation equally invalid. In fact, the continuum approach is invalid for problems with ϵ of order 1 or larger and either microscopic or mesoscopic modeling would be needed in this case. On the other hand, in the limit $\lambda \to \infty$, Eq. (35) approaches the pure advection equation. In fact, in solving the species transport problem based on the Boltzmann equation, the advection and dispersion will not be treated as separate components of the flux term. Nevertheless, whenever the Boltzmann equation is solved with finite λ, the diffusional dissipation of a sharp concentration front will be accounted for.

4. Discretization of the BGK Boltzmann equation

The solution for a concentration field based on the BGK Boltzmann equation now requires integration of Eq. (22) to obtain Eq. (23), and then a direct solution of Eq. (23). However, this procedure is complicated by the facts that f is not known and that solution of the resulting differential equation is complicated by geometric effects and the velocity field. To overcome these obstacles, two important alterations are made to Eq. (22). Firstly, the unknown function f is expressed in terms of the known function q based on the expansions presented previously. This may be done in a variety of ways. Typically, a region of study is discretized into a number of blocks or elements. Then within each element, an equilibrium expression for is q applied. Variation of q within the element can be allowed using polynomials to whatever degree desired. Issues relating to discontinuities in f at the element boundaries require special attention. Secondly, the differential form of Eq. (22) is approximated in a difference form. Thus, performance of the integrations leads to a discrete analog of Eq. (23). In the present section, issues relating to the discretization and approximation of f will be examined.

Consider the grid in Fig. 1, which shows a portion of a region of interest. The discussion here will center on the formulations of the approximations to f associated with the grid box centered at (x_i, y_j) with boundaries at $x_{i-1/2}, y_{j+1/2}, x_{i+1/2}$, and $y_{j-1/2}$. The subscript i will be used to indicate the x-coordinates and the subscript j the y-coordinates. In particular it is important to obtain

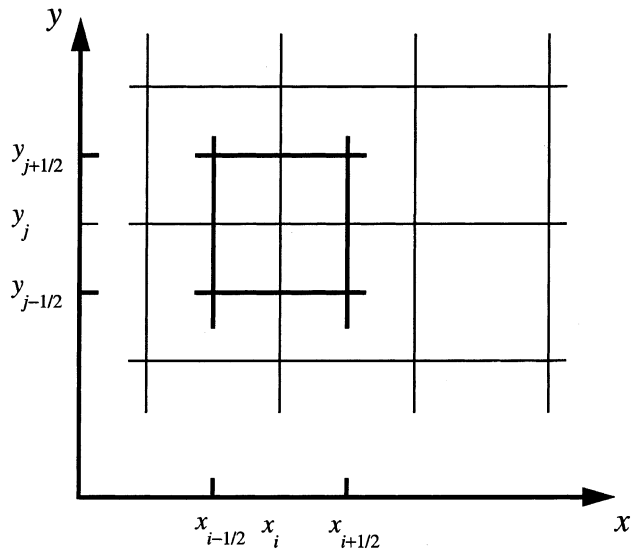

Fig. 1. A two-dimensional computational cell and its interfaces.

expressions for the distribution functions on the boundary of the grid block because the total mass fluxes at the cell boundaries are obtained from the moments of f. Here, the exposition will focus exclusively on the boundary at $x_{i+1/2}$. Totally analogous manipulations apply to the other boundaries.

Consider the solution to Eq. (15a) along a characteristic extending from the location $(X_{i+1/2}, Y_j, t^n)$ and terminating at the interface $(x_{i+1/2}, y_j, t)$. From Eq. (15a)

$$f(\mathbf{x}_{i+1/2,j}, t) = f(\mathbf{X}_{i+1/2,j}, t^n)\mathrm{e}^{-(t-t^n)/\tau} + \frac{1}{\tau}\int_{t^n}^{t} \bar{q}[\mathbf{x}(\beta), \beta]\mathrm{e}^{-(t-\beta)/\tau}\,\mathrm{d}\beta, \tag{37a}$$

where for convenience, the dependence of the distribution function on $\mathbf{c}$ is not explicitly indicated and deviations of $\mathbf{F}/m$ in Eq. (15c) from zero have been ignored for now (such that the particles move with constant speed along straight paths). The case of non-zero $\mathbf{F}$ is discussed in Appendix A. The function, q that appears in the integral is an approximation to q modified so that it is C^0 continuous at the interface. This approximation will be developed subsequently. Note that the starting location for the characteristic is a function of time and is obtained by integration of Eq. (15b) as

$$\mathbf{X}_{i+1/2,j}(t) = \mathbf{x}_{i+1/2,j} - \mathbf{c}(t - t^n) \tag{37b}$$

and the particle trajectories are given by

$$\mathbf{x}(\beta) = \mathbf{X}_{i+1/2,j}(t) + \mathbf{c}(\beta - t^n). \tag{37c}$$

To obtain the form for $f(\mathbf{x}_{i+1/2,j}, t)$, both $f(\mathbf{X}_{i+1/2,j}, t^n)$ and $\bar{q}[\mathbf{x}(\beta), \beta]$ must be known. They will be evaluated in Sections 4.1. and 4.2.

4.1. Evaluation of $f(\mathbf{X}_{i+1/2,j}, t^n)$

The function $f(\mathbf{X}_{i+1/2,j}, t^n)$, where $\mathbf{X}_{i+1/2,j} = \mathbf{X}_{i+1/2,j}(t)$, may be obtained from a Taylor series expansion according to

$$f(\mathbf{X}_{i+1/2,j}, t^n) = q^n_{i+1/2^-,j} + (\nabla q)^n_{i+1/2^-,j} \cdot (\mathbf{X}_{i+1/2,j} - \mathbf{x}_{i+1/2,j}) \quad \text{for} \quad X_{i+1/2} \leqslant x_{i+1/2} \tag{38a}$$

and

$$f(\mathbf{X}_{i+1/2,j}, t^n) = q^n_{i+1/2^+,j} + (\nabla q)^n_{i+1/2^+,j} \cdot (\mathbf{X}_{i+1/2,j} - \mathbf{x}_{i+1/2,j}) \quad \text{for} \quad X_{i+1/2} > x_{i+1/2}, \tag{38b}$$

where use has been made of the assumption that within a cell the equilibrium situation applies such that $f = q$ while discontinuities in f at the boundary of the cell account for disequilibrium. The superscripts "+" and "−" on the subscripts indicate on which side of the discontinuity at $i + 1/2$ the functions are being evaluated. Substitution of Eq. (15b) into these expressions yields

$$f(\mathbf{X}_{i+1/2,j}, t^n) = q^n_{i+1/2^-,j} - (\nabla q)^n_{i+1/2^-,j} \cdot \mathbf{c}(t - t^n) \quad \text{for} \quad X_{i+1/2} \leqslant x_{i+1/2} \tag{39a}$$

and

$$f(\mathbf{X}_{i+1/2,j}, t^n) = q^n_{i+1/2^+,j} - (\nabla q)^n_{i+1/2^+,j} \cdot \mathbf{c}(t - t^n) \quad \text{for} \quad X_{i+1/2} > x_{i+1/2}. \tag{39b}$$

The expressions for $f(\mathbf{X}_{i+1/2,j}, t^n)$ provided in Eqs. (39a) and (39b) may be combined into a single expression by making use of the Heaviside step function such that

$$f(\mathbf{X}_{i+1/2,j}, t^n) = H(c_x)\left\{q^n_{i+1/2^-,j} - (\nabla q)^n_{i+1/2^-,j} \cdot \mathbf{c}(t - t^n)\right\} + [1 - H(c_x)]\left\{q^n_{i+1/2^+,j} - (\nabla q)^n_{i+1/2^+,j} \cdot \mathbf{c}(t - t^n)\right\}, \tag{40}$$

where the Heaviside step function $H(c_x)$ is such that

$$H(c_x) = 1 \quad \text{for } c_x \geqslant 0, \tag{41a}$$

$$H(c_x) = 0 \quad \text{for } c_x < 0. \tag{41b}$$

The functional form of q is provided as Eq. (16). The gradients of q may be calculated, in general, from this expression as

$$\nabla q = q\left[\frac{1}{C}\nabla C + 2\lambda\nabla\mathbf{v}\cdot(\mathbf{c} - \mathbf{v}) + \left(\frac{1}{\lambda} - |\mathbf{c} - \mathbf{v}|^2\right)\nabla\lambda\right]. \tag{42}$$

Note that determination of ∇q requires a knowledge of the concentration, velocity, and pressure fields, either from calculation or as a specified function. Furthermore, the evaluation of q and its derivatives at the boundary of a cell based on the calculated or specified values of $C, \mathbf{v}$, and λ at the center of a cell is not unique. In the example to be presented here, the velocity and

pressure fields are specified as analytic continuous functions in space. The expressions used to evaluate C and ∇C at the boundary of the cell from calculated values C of at the cell centers are given in Appendix B. The technique presented there may also be applied to the velocity and pressure fields in more complex cases where they are only known discretely.

4.2. Evaluation of $\bar{q}[\mathbf{x}(\beta),\beta]$

The calculation of this C^0 continuous function begins with the Taylor series expansion of second-order such that

$$\bar{q}[\mathbf{x},\beta] = \bar{q}^n_{i+1/2,j} + (\nabla\bar{q})^n_{i+1/2^-,j}\cdot(\mathbf{x}-\mathbf{x}_{i+1/2,j}) + \left(\frac{\partial\bar{q}}{\partial\beta}\right)^n_{i+1/2,j}(\beta-t^n) \quad \text{for } x\leqslant x_{i+1/2} \tag{43a}$$

and

$$\bar{q}[\mathbf{x},\beta] = \bar{q}^n_{i+1/2,j} + (\nabla\bar{q})^n_{i+1/2^+,j}\cdot(\mathbf{x}-\mathbf{x}_{i+1/2,j}) + \left(\frac{\partial\bar{q}}{\partial\beta}\right)^n_{i+1/2,j}(\beta-t^n) \quad \text{for } x> x_{i+1/2}, \tag{43b}$$

where the function $\bar{q}$ is defined analogously to q in Eq. (16) with

$$\bar{q} = \bar{C}\frac{\lambda}{\pi}\exp[-\lambda|\mathbf{c}-\bar{\mathbf{v}}|^2] \tag{43c}$$

with derivatives analogous to those in Eq. (42)

$$\nabla\bar{q} = \bar{q}\left[\frac{1}{\bar{C}}\nabla\bar{C} + 2\lambda\nabla\bar{\mathbf{v}}\cdot(\mathbf{c}-\bar{\mathbf{v}}) + \left(\frac{1}{\bar{\lambda}}-|\mathbf{c}-\bar{\mathbf{v}}|^2\right)\nabla\bar{\lambda}\right] \tag{43d}$$

and

$$\frac{\partial\bar{q}}{\partial\beta} = \bar{q}\left[\frac{1}{\bar{C}}\frac{\partial\bar{C}}{\partial\beta} + 2\lambda\frac{\partial\bar{\mathbf{v}}}{\partial\beta}\cdot(\mathbf{c}-\bar{\mathbf{v}})\right]. \tag{43e}$$

In these equations, $\bar{C}$ (and $\bar{\mathbf{v}}$ and $\bar{\lambda}$, if not specified as continuous fields) is an interpolant of C (and $\bar{\mathbf{v}}$ and $\bar{\lambda}$) based on the values of C at the cell centers developed such that it is C^0 continuous at the cell boundaries. The procedures used here to calculate these interpolants are given in Appendix C. The derivatives of $\bar{q}$ with respect to y and t will be continuous at $x_{i+1/2,j}$ but, since q is only C^0 continuous, its first derivative in the direction normal to the boundary of the region (in this case, the x derivative) will be discontinuous. That is the reason for the persistence of the "+" and "−" superscripts in the subscripts of the gradient terms. Eqs. (43a) and (43b) may be combined making use of the Heaviside step function, and the continuity properties of $\bar{q}$ and its derivatives to obtain

$$\bar{q}[\mathbf{x},\beta] = \bar{q}^n_{i+1/2,j} + \left[\frac{\partial\bar{q}}{\partial y}\right]^n_{i+1/2,j}(y-y_j) + \left(\frac{\partial\bar{q}}{\partial\beta}\right)^n_{i+1/2,j}(\beta-t^n) + \left\{H(c_x)\left[\frac{\partial\bar{q}}{\partial x}\right]^n_{i+1/2^-,j} + [1-H(c_x)]\left[\frac{\partial\bar{q}}{\partial x}\right]^n_{i+1/2^+,j}\right\}\times(x-x_{i+1/2}). \tag{44}$$

In the problems studied here, it should be noted that the purpose is exposition of the method in its application to simple problems. Therefore, no numerical calculation is done for the flow field. Due to this, no value of λ has been calculated. Thus, the value of λ employed is obtained from Eq. (36) as

$$\lambda = \frac{\epsilon\hat{\tau}}{2D}, \tag{45}$$

where a physically realistic value of the diffusion coefficient is used and $\epsilon\hat{\tau} = \tau$ is obtained from

$$\tau^n_{i+1/2} = A_1\Delta t + A_2\frac{\left|C^n_{i+1/2^+,j} - C^n_{i+1/2^-,j}\right|}{C^n_{i+1/2^+,j} + C^n_{i+1/2^-,j}}\Delta t \quad \text{for} \quad y\in[y_{j-1/2}, y_{j+1/2}]. \tag{46}$$

The constants A_1 and A_2 are determined from numerical experiment. [13] report that the BGK Boltzmann solution scheme is robust with respect to the choice of these constants. [32] have used values of A_1 and A_2 on the order of 0.01 and 1.0, respectively, when simulating shocks in gas dynamics problems. [7] have used the same values for shallow water calculations. In the calculations performed in the present work, τ was set equal to 200 D.

4.3. Summary of discretization procedure for distribution function

The discretization procedure is directed toward obtaining an approximation for $f(\mathbf{x}_{i+1/2,j},t)$ as found in Eq. (37a). This is achieved making use of the expressions for the terms on the right-hand side of Eq. (37a) as provided by Eqs. (40) and (44). For a cell centered at $\mathbf{x}_{i,j}$, analogous relations may be obtained for $f(\mathbf{x}_{i-1/2,j},t)$, $f(\mathbf{x}_{i,j+1/2},t)$, and $f(\mathbf{x}_{i,j-1/2},t)$. Thus, expressions are provided for each of the distribution functions along the boundary of a cell. It is important to note that by the procedure employed here, a unique value for the distribution at a cell interface is obtained that depends on the information from cells on both sides of each interface. Of further importance is the fact that, in application, the distribution functions are not explicitly calculated. The overall goal is to solve the transport Eq. (23). The discrete form of this equation, derived from the discretization of the Boltzmann equation, is what is solved in the numerical model. This form is based on the integration over the particle velocities of

the distribution functions obtained here. Only these integrals of the distribution functions must be evaluated. At time level n, the values of C and $\mathbf{v}$ are known at the cell centers. The limiter is used to determine these quantities within the cell at t^n . This process of determining the discrete transport equation is referred to as the reconstruction procedure and is described in Section 5.

5. Reconstruction of the transport equation

The numerical formulation of the mesoscopic transport model is based on Eq. (23) integrated in space over each cell of interest (e.g., the cell in Fig. 1) and over time from t^n to t^{n+1}. Integration of Eq. (23) yields

$$C_{i,j}^{n+1} = C_{i,j}^{n} - \int_{t^n}^{t^{n+1}} \frac{(N_x)_{i+1/2,j} - (N_x)_{i-1/2,j}}{\Delta x}\,\mathrm{d}t - \int_{t^n}^{t^{n+1}} \frac{(N_y)_{i,j+1/2} - (N_y)_{i,j-1/2}}{\Delta y}\,\mathrm{d}t, \tag{47}$$

where N_x is the flux in the x-direction and N_y is the flux in the y-direction. These fluxes are obtained as integrals of the distribution functions developed in the last section. For example, at the $x_{i+1/2}$ boundary

$$(N_x)_{i+1/2,j} = \int_{-\infty}^{\infty}\int_{-\infty}^{\infty} c_x f(\mathbf{x}_{i+1/2,j}, t)\,\mathrm{d}c_x\,\mathrm{d}c_y, \tag{48}$$

where the distribution $f(\mathbf{x}_{i+1/2,j}, t)$ is known from the last section. The other terms in the integrals may be developed and evaluated similarly. Thus, all integrations indicated on the right-hand side of Eq. (47) may be performed such that the solution for $C_{i,j}^{n+1}$ is obtained explicitly. The main task, therefore, in the full construction of a solution to the transport equation based on the BGK Boltzmann equation is the manipulations that go into the specification of $f(\mathbf{x}_{i+1/2,j}, t)$.

6. Summary of the solution procedure

The calculations that must be performed are provided in detail in Appendices BCD. It is convenient to summarize the procedure for advancing the solution from t^n to t^{n+1}

1. Start with known values of $C_{i,j}^n$.
2. Determine the derivatives of C within each cell using the flux limiters of Eqs. (56a) and (56b).
3. The derivatives and the values of $C_{i,j}^n$ are used to calculate the values of C^n at the cell boundaries from Eq. (55).
4. The values of $\bar{C}^n$ at the cell interfaces are calculated using equations analogous to Eq. (59).
5. The derivatives of $\bar{C}^n$ within each cell are obtained from equations analogous to (63a) and (63b).
6. Information from steps 4 and 5 is used to calculate the time derivative of $\bar{C}$ at t^n and at the interfaces using expressions such as Eq. (76).
7. The quantities calculated in steps 2–6 are useful in calculating the expressions for the the derivatives of q and $\bar{q}$ needed to calculate f at the interface as in Eq. (37a). The description of this calculation is provided in Eq. (38a)–(44).
8. Finally, from the known values of f at the interfaces, the fluxes can be evaluated for the integrals appearing in Eq. (47) such that the solution for $C_{i,j}^{n+1}$ is obtained.

7. Example calculations

Several transport problems will now be solved for the purpose of demonstrating the effectiveness of the procedure developed here. The model, once developed, is easily applied to complex flow fields and concentration distributions. However, here the focus is on simply described problems that illustrate the attributes of the computational procedure.

7.1. One-dimensional pure advection tests

The first example is the pure advection of a Gaussian concentration profile with a peak value 1 and a standard deviation 264. Fig. 2 shows that both analytical and numerical solutions at time 10,000 s agree well.

The second test demonstrates the one-dimensional advection of a "step" profile. Both analytical and numerical solutions at different times are shown in Fig. 3. This calculation shows that the implemented model is able to handle sharp fronts without introducing overshoots and undershoots. It should be noted that no special treatment of the front is required as the approximation procedure is the same for all points in the system.

7.2. Test of the Leonard problem

[15] has devised a test case that consists of three concentration distributions that are to be advected in

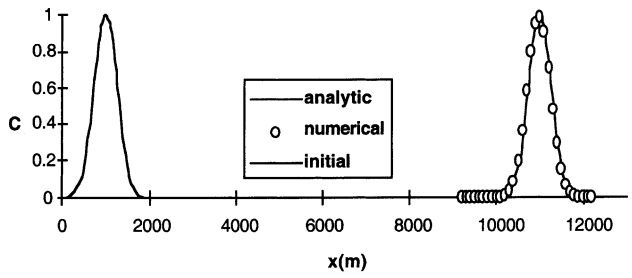

Fig. 2. Pure advection test (solution at $t = 10,000$ s with $u\Delta t/\Delta x = 0.9$, $u = 1.0$ m/s, and $\Delta x = 100$ m.

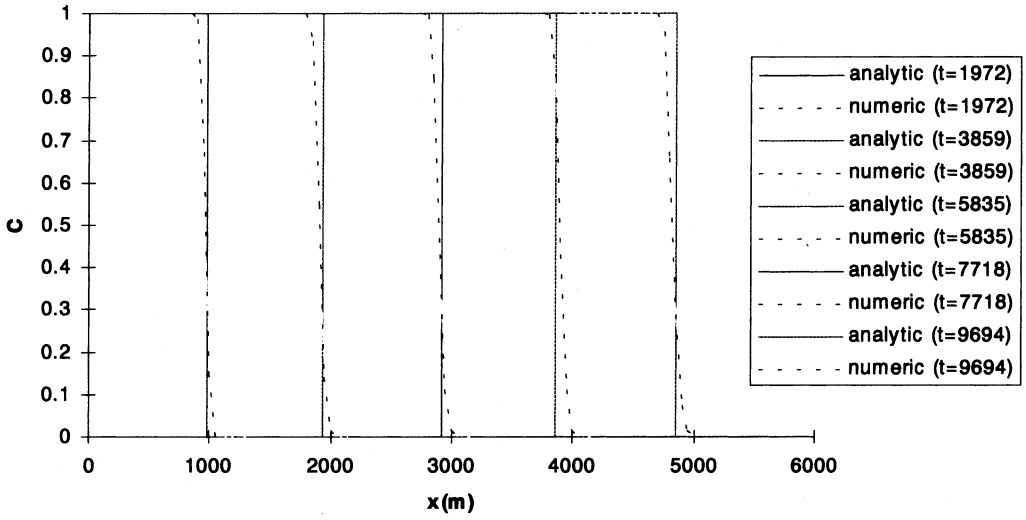

Fig. 3. "Step" test at different times with $u\Delta t/\Delta x = 0.96$, $\Delta x = 50$ m, and $u = 0.5$ m/s.

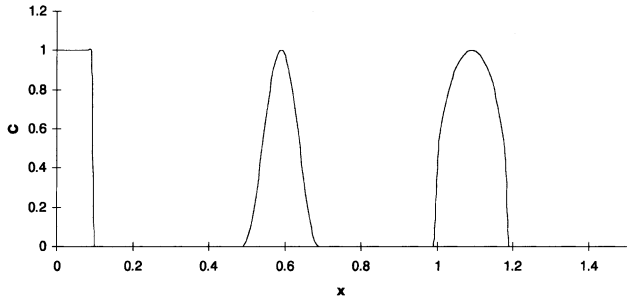

Fig. 4. Initial concentration profile for the Leonard test.

one-dimension. The initial condition is illustrated in Fig. 4. The lead distribution is a semi-ellipse of width $20\Delta x$. The middle distribution is a sine-squared distribution, also of width $20\Delta x$, and the lagging distribution is a sharp front. This initial condition is advected to the right by a normalized speed of 1. The discretization is the same as that used by [15] and parameter values are indicated in the solution plotted in Fig. 5.

To evaluate the performance of the proposed mesoscopic model in comparison with the results obtained by various ULTIMATE schemes, the absolute error e and the waviness error w defined, respectively, by [15] as

$$e = \sum_i |C_{\text{exact},i} - C_{\text{computed},i}| \tag{49}$$

and

$$w = \sum_i |(C_{i+1} - C_i)_{\text{exact}} - (C_{i+1} - C_i)_{\text{computed}}| \tag{50}$$

are employed. Fig. 6 plots the absolute errors in approximating the step (e-STEP), the sine (e-SINE) and the ellipse (e-ELLIPSE) obtained with the mesoscopic model at the second-order position on the abscissa. For comparison, the absolute errors of the second-, third-, fourth-, fifth-, sixth-, seventh-, eighth- and ninth-order ULTIMATE schemes are also plotted versus the order of the scheme. The figure shows: (i) e-STEP of the proposed second-order scheme is the same as that of the

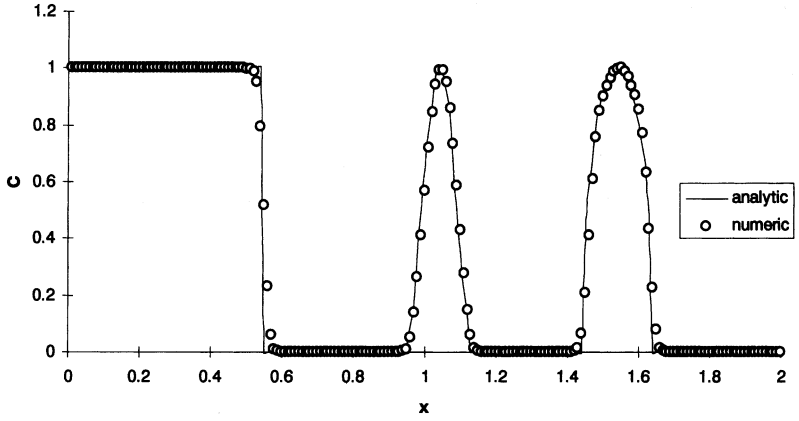

Fig. 5. Analytical and numerical solutions to the Leonard test after 90 time-steps with $u\Delta t/\Delta x = 0.5$, $\Delta x = 0.01$ m, $u = 0.045$ m/s.

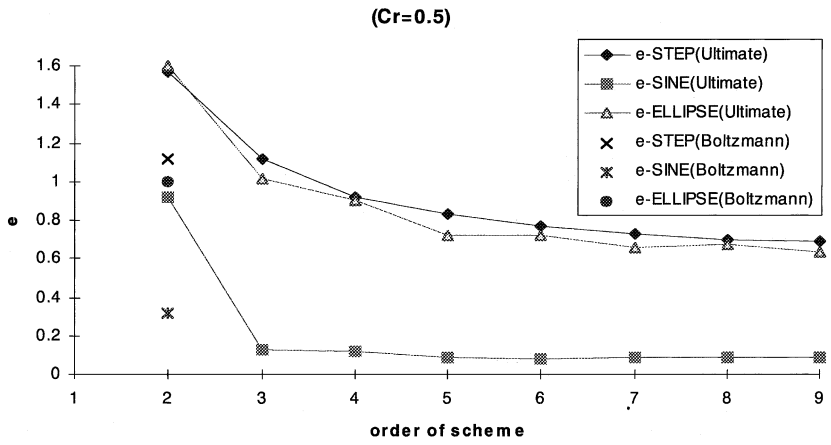

Fig. 6. Comparisons of total absolute errors for Leonard test after 90 time-steps with $u\Delta t/\Delta x = 0.5,\ \Delta x = 0.01$ m, $u = 0.045$ m/s.

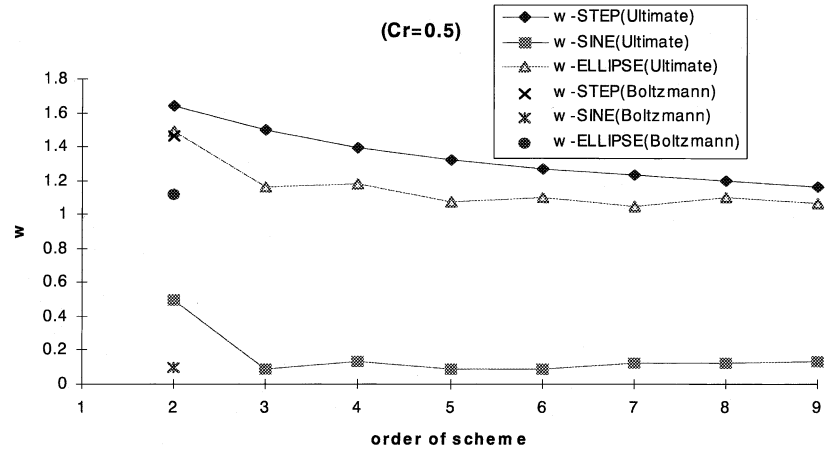

Fig. 7. Comparisons of waviness errors for Leonard test after 90 time-steps with $u\Delta t/\Delta x = 0.5,\ \Delta x = 0.01$ m, $u = 0.045$ m/s.

third-order ULTIMATE scheme; (ii) *e*-ELLIPSE of the proposed scheme is the same as that of the fourth-order ULTIMATE scheme; (iii) *e*-SINE of the proposed scheme is better than that of the second-order ULTIMATE scheme but worse than that of the third-order scheme ULTIMATE scheme; (iv) the absolute error in approximating the whole profile of the proposed second-order scheme is the same as that of the third-order ULTIMATE scheme. Hence, for the same discretization, the proposed second-order model produces the same global absolute error as the third-order ULTIMATE scheme of Leonard.

Fig. 7 shows the waviness errors *w*-STEP, *w*-SINE and *w*-ELLIPSE versus the order of the scheme. It can be seen that: (i) *w*-STEP of the proposed scheme is the same as that of the fourth-order ULTIMATE scheme; (ii) *w*-ELLIPSE of the second-order proposed scheme is better than that of ULTIMATE schemes up to the ninth-order; (iii) *w*-SINE of the second-order proposed scheme is better than that of the ULTIMATE scheme up to the ninth-order. In summary, the absolute error in the mesoscopic model is equivalent to the third-order ULTIMATE scheme and the waviness error in the proposed model is better than that in the ninth-order ULTIMATE scheme.

7.3. Advection–diffusion test

This example is intended to test the capability of the model in handling the advection–diffusion transport under different diffusion strengths. The initial profile is chosen as a Gaussian distribution with the peak value 1 and the standard deviation 264. Fig. 8 shows both analytical and numerical solutions for different Peclet numbers. It can be seen that all the numerical results agree with the analytical results very well.

7.4. Two-dimensional transport tests

The first two-dimensional example tests the capability of the proposed mesoscopic model in handling two-dimensional steep gradients. A cube of base $19\Delta x \times 19\Delta y$ and of height one is advected diagonally. Fig. 9 shows the initial concentration distribution surface and the

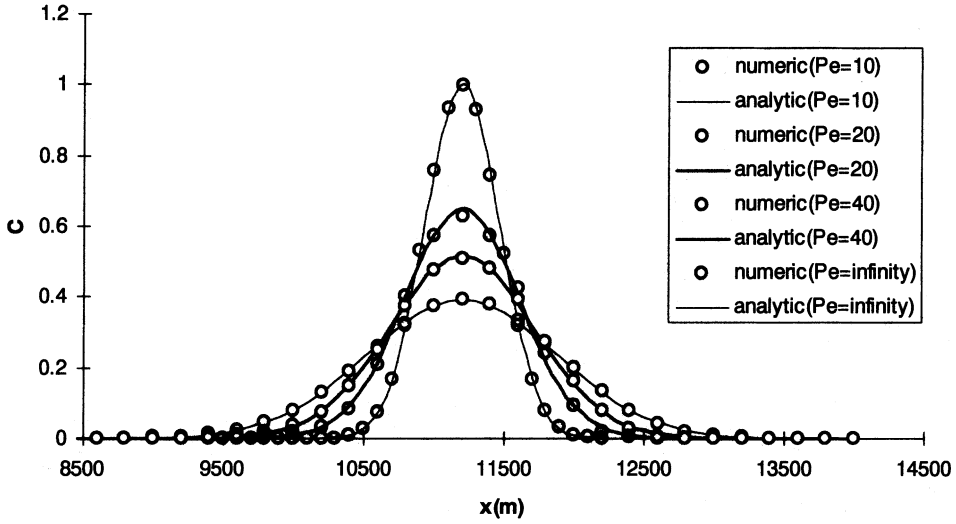

Fig. 8. Advection–diffusion test for transport of a Gaussian distribution after 96 time-steps using different Peclet numbers with $u\Delta t/\Delta x = 0.5,\ \Delta x = 200$ m, $u = 1$ m/s.

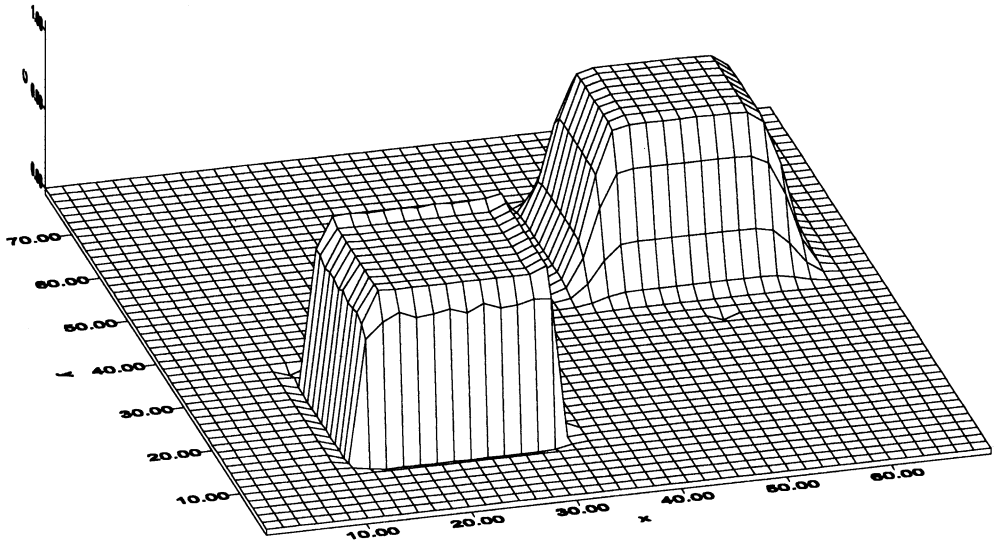

Fig. 9. Two-dimensional advection test with $\Delta x = 1,\ u = v = 1,\ \Delta t = 1$. Initial condition and solution after 30 time-steps.

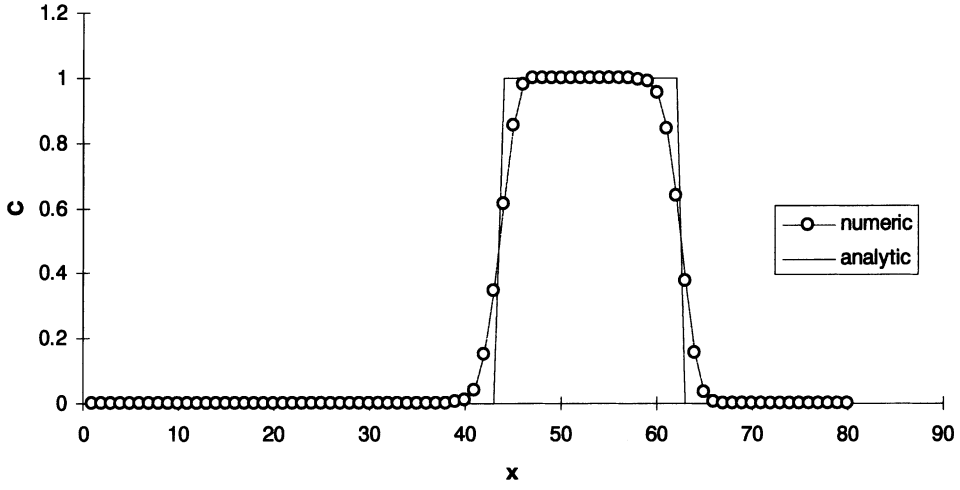

Fig. 10. Comparison of analytical and computed profiles for two-dimensional advection test of Fig. 9 at $y = 50$.

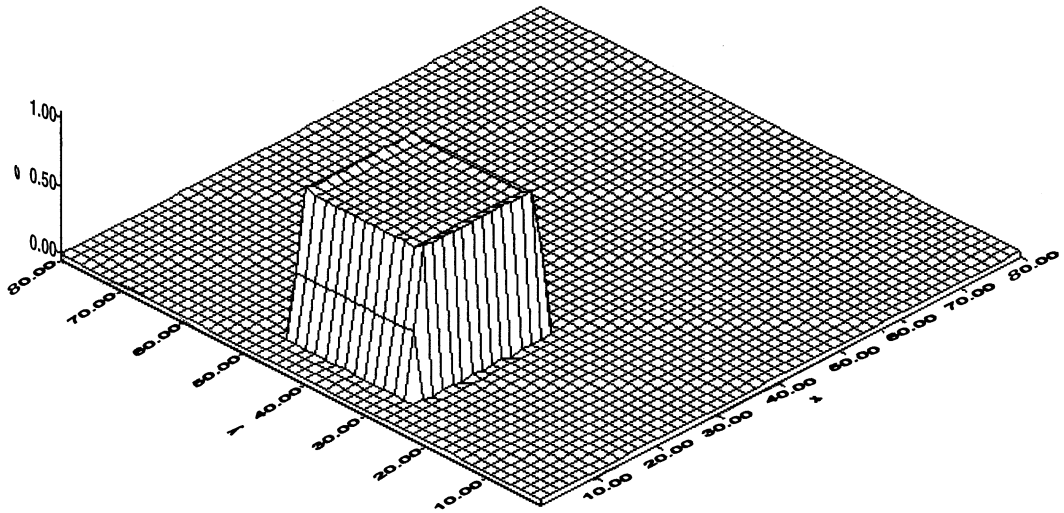

Fig. 11. Initial concentration surface for advection in a rotational flow field. Computational region is a square with side length 80 and $\Delta x = \Delta y = 1$. Concentration square is $19\Delta x \times 19\Delta y$.

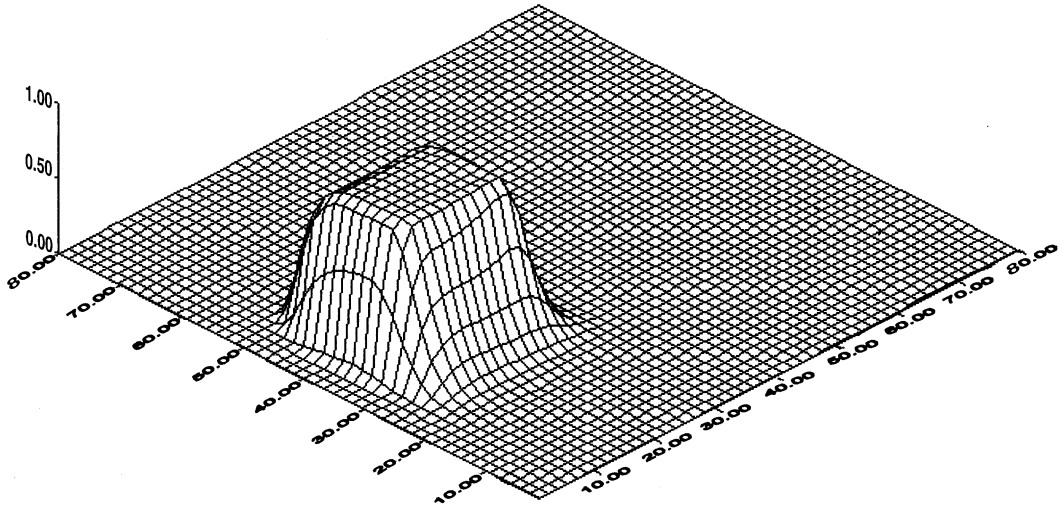

Fig. 12. Predicted concentration surface after one revolution (160 time-steps) from initial condition of Fig. 11.

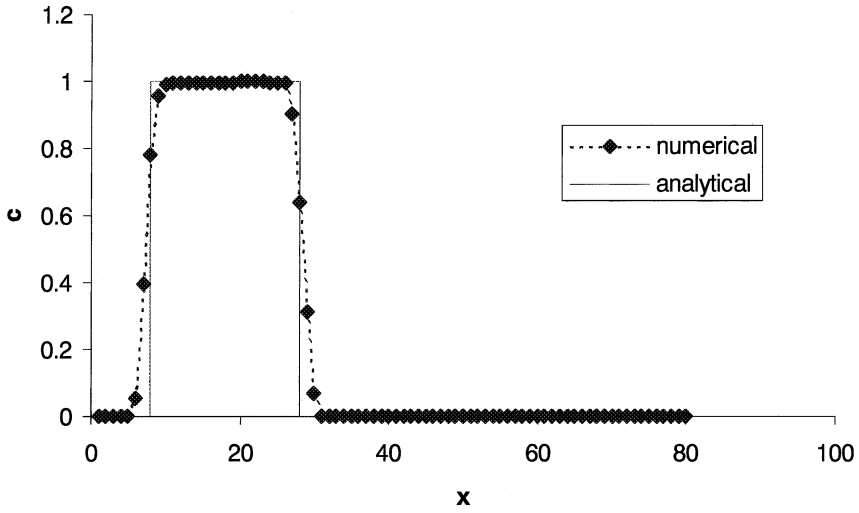

Fig. 13. Comparison of computed profile from Fig. 12 at $y = 40$ with analytical solution.

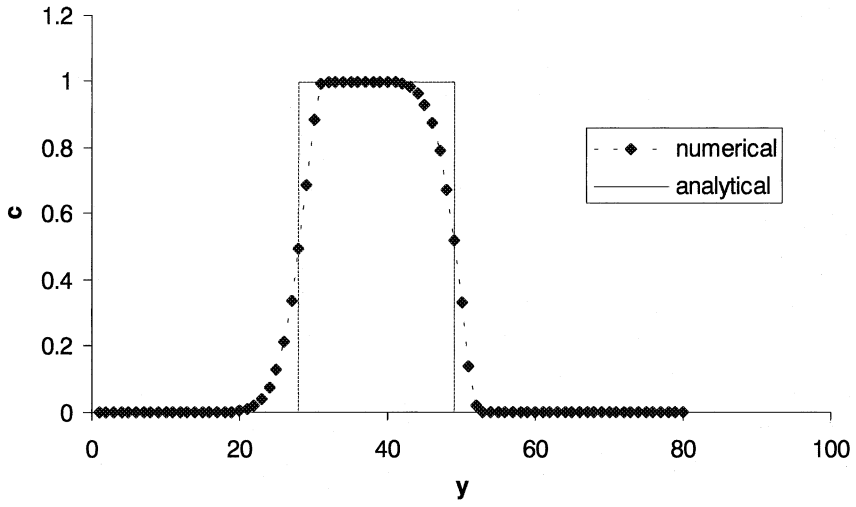

Fig. 14. Comparison of computed profile from Fig. 12 at $x = 20$ with analytical solution.

surface after 30 time-steps. It indicates that the mesoscopic model gives stable and quite satisfactory results. Fig. 10 compares a computed and analytical cross-section of the concentration profile and demonstrates the high resolution obtained for the discontinuity.

The second two-dimensional example tests the mesoscopic model in simulating a two-dimensional steep gradient profile transported in a non-uniform flow field. The test domain is an $80\Delta x \times 80\Delta y$ square. The velocity field is a counter-clockwise circular flow similar to that of a rigid body rotating about its center. The angular speed is $\pi/80$, and one complete revolution requires 160 time-steps. The initial concentration distribution surface is shown in Fig. 11, with a square base of $20\Delta x \times 20\Delta y$ and height one, the center of which is located at $(\mathbf{x} = 20\Delta x \times 20\Delta y)$. Since diffusion is not included, the concentration distribution after a complete revolution should coincide with the initial concentration distribution. Fig. 12 shows the computed concentration distribution surface after a complete revolution. Figs. 13 and 14 compare the computed concentration profiles with analytical solutions and demonstrate the resolution obtained for the discontinuous profile.

8. Conclusion

In this paper, a mesoscopic model for the advection–diffusion contaminant transport is proposed based on the kinetic theory. It utilizes BGK collisional Boltzmann equation as a starting point. The finite volume method is used to establish the second-order mesoscopic level based numerical model. The mesoscopic model has a number of attractive features. It satisfies the entropy condition and can be easily extended to multi-dimensional cases. In addition, in the BGK model, the diffusion term is represented by a simple algebraic difference term rather than a second-order partial derivative term, which much simplifies the discretization and prevents the numerical oscillation. Another outstanding attribute of the mesoscopic model is that the convection term in the BGK Boltzmann equation is linear. Numerical results obtained for a range of advection–diffusion transport problems, including one- and two-dimensional pure advection transport and advection–diffusion transport, have been compared with analytical solutions and numerical solutions obtained by other schemes. The comparisons show the high accuracy, stability, and robustness of the proposed mesoscopic model.

Acknowledgements

This work was supported, in part, by the Research Grants Council (RGC) of Hong Kong under project number HKUST718/96E.

Appendix A. Non-zero net external force

If the resultant of all external forces is not zero (i.e., $\mathbf{F} \neq 0$), then the derivation of the discrete Boltzmann equation from Eq. (37a) to (44) is altered. An approximate solution for the distribution function at interface $i + 1/2$ is obtained using either operator splitting or using approximate particle paths determined through numerical integration of the Eqs. (15b) and (15c). Both approaches are discussed in this appendix.

A.1. Operator splitting when $\mathbf{F} \neq 0$

Operator splitting [10,16,35] may be used to rewrite the Boltzmann equation as follows:

$$\frac{\partial f^*}{\partial t} + \mathbf{c}\cdot\nabla f^* = \frac{\bar{q} - f^*}{\tau} \text{ with initial condition}$$
$$f^*(\mathbf{x},\mathbf{c},t^n) = f(\mathbf{x},\mathbf{c},t^n), \tag{51a}$$

$$\frac{\partial f^{**}}{\partial t} + \frac{\mathbf{F}}{m}\cdot\frac{\partial f^{**}}{\partial \mathbf{c}} = 0 \text{ with initial condition}$$
$$f^{**}(\mathbf{x},\mathbf{c},t^n) = f^*(\mathbf{x},\mathbf{c},t) \tag{51b}$$

for $t \in [t^n, t^{n+1}]$. This splitting has been used by [7] for transient open channel flow problems to advantage.

Eq. (51a) is identical to the Boltzmann equation with $\mathbf{F} = 0$, and its solution is identical to Eq. (37a) and requires the same manipulations as provided in the text for calculation of that solution. Eq. (51b) may be expressed in the characteristic form useful for its solution

$$\frac{\mathrm{d}f^{**}}{\mathrm{d}t} = 0 \tag{52a}$$

subject to

$$\frac{\mathrm{d}\mathbf{c}}{\mathrm{d}t} = \frac{\mathbf{F}}{m}. \tag{52b}$$

The solution to this equation pair at the cell interface $i+1/2$ is

$$f^{**}[\mathbf{x}_{i+1/2,j},\mathbf{c},t] = f^*[\mathbf{x}_{i+1/2,j},\mathbf{c},t], \tag{53a}$$

where

$$\mathbf{c} = \mathbf{c}^n + \int_{t^n}^{t} \frac{\mathbf{F}}{m}\,\mathrm{d}t. \tag{53b}$$

Since the expression for $\mathbf{c}$ that appears in the right-hand side of Eq. (53a) contains a time integral of the net external force, an approximate quadrature method can be employed. [7] have found that a first-order integration was sufficient for the study of transient open channel flows such as dam break problems.

A.2. No operator splitting when $\mathbf{F} \neq 0$

When no operator splitting is employed with $\mathbf{F} \neq 0$, Eqs. (37a) and (37c) are still employed as the solution for $f(\mathbf{x}_{i+1/2,j},t)$, but Eq. (37b) is replaced by

$$\mathbf{X}_{i+1/2,j}(t) = \mathbf{x}_{i+1/2,j} - \mathbf{c}^n(t-t^n) - \int_{t^n}^{t}\int_{t^n}^{\beta} \frac{\mathbf{F}}{m}\,\mathrm{d}\gamma\,\mathrm{d}\beta, \tag{54}$$

where β and γ are dummy variables. To determine the particle paths, an approximate quadrature method must be selected for the integral that appears in this equation. Then the solution provided by Eq. (37a) and the method for evaluating this solution are employed as described when $\mathbf{F} = 0$ with the expression for $\mathbf{X}_{i+1/2,j}(t)$ given by Eq. (54) rather than Eq. (37b).

Appendix B. Evaluation of C and ∇C at cell boundaries

The equilibrium distribution function q, as given in Eq. (16), and its gradient, as given in Eq. (42) must be evaluated at the boundaries of the computational cell in Eq. (40). To do these evaluations, C, $\mathbf{v}$, and λ, which are known at the cell centers, must be interpolated to the cell boundaries. In fact, for the simple examples demonstrated here, the velocity fields are specified at all points in space and the pressure field is a constant so the only function that actually must be treated is the concentration field.

Here, within a cell centered at $\mathbf{x}_{i,j}$, the concentration profile will be represented as the second-order Taylor series

$$C^n(\mathbf{x}) = C^n_{i,j} + (\mathbf{x} - \mathbf{x}_{i,j})\cdot(\nabla C)^n_{i,j}. \tag{55}$$

The derivative functions are obtained using the monotonic upstream centered scheme for conservation laws (MUSCL) slope limiter introduced by van Leer [27]

$$\left(\frac{\partial C}{\partial x}\right)_{i,j} = \frac{\mathrm{sgn}(\Delta_x C_{i,j}) + \mathrm{sgn}(\nabla_x C_{i,j})}{2\Delta x} \times \min(|\delta_x C_{i,j}|, |\Delta_x C_{i,j}|, |\nabla_x C_{i,j}|), \tag{56a}$$

$$\left(\frac{\partial C}{\partial y}\right)_{i,j} = \frac{\mathrm{sgn}(\Delta y C_{i,j}) + \mathrm{sgn}(\nabla y C_{i,j})}{2\Delta y} \times \min(|\delta_y C_{i,j}|, |\Delta_y C_{i,j}|, |\nabla_y C_{i,j}|) \tag{56b}$$

where

$$\Delta_x C_{i,j} = C_{i+1,j} - C_{i,j}, \tag{57a}$$

$$\nabla_x C_{i,j} = C_{i,j} - C_{i-1,j}, \tag{57b}$$

$$\delta_x C_{i,j} = \frac{1}{2}(\Delta_x C_{i,j} + \nabla_x C_{i,j}) = \frac{1}{2}(C_{i+1,j} - C_{i-1,j}), \tag{57c}$$

$$\Delta_y C_{i,j} = C_{i,j+1} - C_{i,j}, \tag{57d}$$

$$\nabla_y C_{i,j} = C_{i,j} - C_{i,j-1}, \tag{57e}$$

$$\delta_y C_{i,j} = \frac{1}{2}(\Delta_y C_{i,j} + \nabla_y C_{i,j}) = \frac{1}{2}(C_{i,j+1} - C_{i,j-1}). \tag{57f}$$

The approximation used here results in derivatives that are constant within a cell. The velocity fields for the examples are provided exactly and thus may be evaluated exactly. Therefore, all the information is available so that a discrete approximation to ∇q is obtained using Eq. (42) and all the items in Eq. (40) will be known.

Appendix C. Evaluation of and its derivatives

The manipulations in the preceding appendix provide an expression for C within a cell. However, at a cell boundary, the value of C will depend on the direction of approach to the boundary. In Eqs. (43a)–(43e) a unique

value of $\bar{C}$ is needed. This is obtained from the values of C in the elements adjacent to the boundary as follows.

If the boundary of interest is at $x_{i+1/2}$, the particle movements toward this boundary will occur from the adjacent cells depending on the particle velocities. Thus, the concentration at the boundary may be defined making use of the distribution functions for those cells as

$$\bar{C}^n_{i+1/2,j} = \int_{-\infty}^{\infty}\int_{-\infty}^{\infty}\Big\{H(c_x)q^n_{i+1/2^-,j} + [1-H(c_x)]q^n_{i+1/2^+,j}\Big\}\,\mathrm{d}c_x\,\mathrm{d}c_y \tag{58a}$$

or

$$\bar{C}^n_{i+1/2,j} = \int_{-\infty}^{\infty}\int_{0}^{\infty} q^n_{i+1/2^-,j}\mathrm{d}c_x\mathrm{d}c_y + \int_{-\infty}^{\infty}\int_{-\infty}^{0} q^n_{i+1/2^+,j}\,\mathrm{d}c_x\,\mathrm{d}c_y. \tag{58b}$$

Evaluation of the integrals based on the tabulated forms in Appendix D yields

$$\bar{C}^n_{i+1/2,j} = \left\{\frac{C}{2}[\mathrm{erfc}(-u\sqrt{\lambda})]\right\}^n_{i+1/2^-,j} + \left\{\frac{C}{2}[\mathrm{erfc}(u\sqrt{\lambda})]\right\}^n_{i+1/2^+,j}, \tag{59}$$

where erfc is the complementary error function.

$$\mathrm{erfc}(\eta) = \frac{2}{\sqrt{\pi}}\int_{\eta}^{\infty}\exp(-r^2)\,\mathrm{d}r. \tag{60}$$

The derivation in Appendix B provides the information needed to calculate C, u, and λ (a surrogate for the pressure) at the two sides of the cell boundary. Thus, $\bar{C}$ is a weighted average of the values on the two sides of the boundary. If a continuous flow field is specified, then there will be no need to calculate an approximate velocity at the boundary of the cell. However, if the field is calculated and not continuous, then the appropriate values for $\bar{u}$ and $\bar{v}$ can be obtained analogously to Eq. (58b) by including c_x and c_y, respectively, in the integrand. This yields

$$(\bar{C}\bar{u})_{i+1/2,j} = \left\{\frac{C}{2}\left[u\,\mathrm{erfc}(-u\sqrt{\lambda}) + \frac{\mathrm{e}^{-\lambda u^2}}{\sqrt{\pi\lambda}}\right]\right\}^n_{i+1/2^-,j} + \left\{\frac{C}{2}\left[u\,\mathrm{erfc}(u\sqrt{\lambda}) - \frac{\mathrm{e}^{-\lambda u^2}}{\sqrt{\pi\lambda}}\right]\right\}^n_{i+1/2^+,j}, \tag{61}$$

$$(\bar{C}\bar{v})_{i+1/2,j} = \left\{\frac{Cv}{2}[\mathrm{erfc}(-u\sqrt{\lambda})]\right\}^n_{i+1/2^-,j} + \left\{\frac{Cv}{2}[\mathrm{erfc}(u\sqrt{\lambda})]\right\}^n_{i+1/2^+,j}. \tag{62}$$

The derivative of $\bar{C}$ with respect to the direction normal to a cell boundary is easily obtained from the discrete expression, for example

$$\left[\frac{\partial\bar{C}}{\partial x}\right]_{i+1/2^-,j} = \frac{\bar{C}_{i+1/2,j} - C_{i,j}}{x_{i+1/2,j} - x_{i,j}}, \tag{63a}$$

$$\left[\frac{\partial\bar{C}}{\partial x}\right]_{i+1/2^+,j} = \frac{C_{i+1,j} - \bar{C}_{i+1/2,j}}{x_{i+1,j} - x_{i+1/2,j}}. \tag{63b}$$

The derivatives of $\bar{C}$ and $\bar{\mathbf{v}}$ with respect to the coordinate tangential to the boundary and β are obtained as simple extensions of their definitions. For example, based on Eq. (58b)

$$\left[\frac{\partial\bar{C}}{\partial y}\right]^n_{i+1/2,j} = \int_{-\infty}^{\infty}\int_{0}^{\infty}\left[\frac{\partial q}{\partial y}\right]^n_{i+1/2^-,j}\mathrm{d}c_x\,\mathrm{d}c_y + \int_{-\infty}^{\infty}\int_{-\infty}^{0}\left[\frac{\partial q}{\partial y}\right]^n_{i+1/2^+,j}\mathrm{d}c_x\,\mathrm{d}c_y, \tag{64}$$

which may be evaluated directly using the tabulated integrals in Appendix D as

$$\left[\frac{\partial\bar{C}}{\partial y}\right]^n_{i+1/2,j} = \left\{\frac{\partial}{\partial y}\left[\frac{C}{2}\mathrm{erfc}(-\sqrt{\lambda}u)\right]\right\}^n_{i+1/2^-,j} + \left\{\frac{\partial}{\partial y}\left[\frac{C}{2}\mathrm{erfc}(\sqrt{\lambda}u)\right]\right\}^n_{i+1/2^-,j}. \tag{65}$$

The derivatives of C, u, and λ on the right-hand side of Eq. (65) are approximated as in Appendix B.

To evaluate the derivative of $\bar{q}$ with respect to time, as in Eqs. (43a) and (43b), the derivative of $\bar{C}$ with respect to time must be known in Eq. (43e). The calculation of this term is more complex than the calculation of the spatial derivatives of $\bar{C}$.

Begin by substituting Eq. (40) into Eq. (37a) to obtain

$$\begin{aligned} f(\mathbf{x}_{i+1/2,j},t) = {} & H(c_x)\Big\{q^n_{i+1/2^-,j} - (\nabla q)^n_{i+1/2^-,j}\cdot\mathbf{c}(t-t^n)\Big\}\\ & \times \mathrm{e}^{-(t-t^n)/\tau} + [1-H(c_x)]\\ & \times\Big\{q^n_{i+1/2^+,j} - (\nabla q)^n_{i+1/2^+,j}\cdot\mathbf{c}(t-t^n)\Big\}\\ & \times \mathrm{e}^{-(t-t^n)/\tau} + \frac{1}{\tau}\int_{t^n}^{t}\bar{q}[\mathbf{x}(\beta),\beta]\mathrm{e}^{-(t-\beta)/\tau}\,\mathrm{d}\beta. \end{aligned} \tag{66}$$

Now substitute the particle trajectory given by Eq. (37c) into Eq. (44) to obtain

$$\begin{aligned} \bar{q}[\mathbf{x},\beta] = {} & \bar{q}^n_{i+1/2,j} + \left[\frac{\partial\bar{q}}{\partial y}\right]^n_{i+1/2,j} c_y(\beta-t)\\ & + \left(\frac{\partial\bar{q}}{\partial\beta}\right)^n_{i+1/2,j}(\beta-t^n) + \left\{H(c_x)\left[\frac{\partial\bar{q}}{\partial x}\right]^n_{i+1/2^-,j}\right.\\ & \left. + [1-H(c_x)]\left[\frac{\partial\bar{q}}{\partial x}\right]^n_{i+1/2^+,j}\right\}c_x(\beta-t). \end{aligned} \tag{67}$$

Then substitution of Eq. (67) into Eq. (66) yields the expression

$$
\begin{aligned}
&f(\mathbf{x}_{i+1/2,j},t)\\
&\quad=H(c_x)\left\{q^n_{i+1/2^-,j}-(\nabla q)^n_{i+1/2^-,j}\cdot\mathbf{c}(t-t^n)\right\}\mathrm{e}^{-(t-t^n)/\tau}\\
&\qquad+[1-H(c_x)]\left\{q^n_{i+1/2^+,j}-(\nabla q)^n_{i+1/2^+,j}\cdot\mathbf{c}(t-t^n)\right\}\mathrm{e}^{-(t-t^n)/\tau}\\
&\qquad+\frac{1}{\tau}\int_{t^n}^{t}\bar{q}^n_{i+1/2,j}\mathrm{e}^{-(t-\beta)/\tau}\,\mathrm{d}\beta+\frac{1}{\tau}\int_{t^n}^{t}\left[\frac{\partial\bar{q}}{\partial y}\right]^n_{i+1/2,j}\\
&\qquad\times c_y(\beta-t)\mathrm{e}^{-(t-\beta)/\tau}\,\mathrm{d}\beta+\frac{1}{\tau}\int_{t^n}^{t}\left(\frac{\partial\bar{q}}{\partial\beta}\right)^n_{i+1/2,j}\\
&\qquad\times(\beta-t^n)\mathrm{e}^{-(t-\beta)/\tau}\,\mathrm{d}\beta+\frac{1}{\tau}\int_{t^n}^{t}\left\{H(c_x)\left[\frac{\partial\bar{q}}{\partial x}\right]^n_{i+1/2^-,j}\right.\\
&\qquad\left.+[1-H(c_x)]\left[\frac{\partial\bar{q}}{\partial x}\right]^n_{i+1/2^+,j}\right\}c_x(\beta-t)\mathrm{e}^{-(t-\beta)/\tau}\,\mathrm{d}\beta.
\end{aligned}
\tag{68}
$$

Evaluation of the indicated integrals then produces

$$
\begin{aligned}
&f(\mathbf{x}_{i+1/2,j},t)\\
&\quad=H(c_x)\left\{q^n_{i+1/2^-,j}-(\nabla q)^n_{i+1/2^-,j}\cdot\mathbf{c}\kappa\tau\right\}\mathrm{e}^{-k}\\
&\qquad+[1-H(c_x)]\left\{q^n_{i+1/2^+,j}-(\nabla q)^n_{i+1/2^+,j}\cdot\mathbf{c}\kappa\tau\right\}\mathrm{e}^{-\kappa}\\
&\qquad+\bar{q}^n_{i+1/2,j}[1-\mathrm{e}^{-\kappa}]+\left[\frac{\partial\bar{q}}{\partial y}\right]^n_{i+1/2,j}c_y\tau[\kappa\mathrm{e}^{-\kappa}-(1-\mathrm{e}^{-\kappa})]\\
&\qquad+\left[\frac{\partial\bar{q}}{\partial t}\right]^n_{i+1/2,j}\tau[\kappa-(1-\mathrm{e}^{-\kappa})]+\left\{H(c_x)\left[\frac{\partial\bar{q}}{\partial x}\right]^n_{i+1/2^-,j}\right.\\
&\qquad\left.+[1-H(c_x)]\left[\frac{\partial\bar{q}}{\partial x}\right]^n_{i+1/2^+,j}\right\}c_x\tau[\kappa\mathrm{e}^{-\kappa}-(1-\mathrm{e}^{-\kappa})],
\end{aligned}
\tag{69}
$$

where $\kappa=(t-t^n)/\tau$. Eq. (44) may be used to obtain an expression for $q(\mathbf{x}_{i+1/2,j},t)$, which will be continuous at the interface as

$$
\bar{q}[\mathbf{x}_{i+1/2,j},t]=\bar{q}^n_{i+1/2,j}+\frac{\partial\bar{q}^n}{\partial t}_{i+1/2,j}\tau\kappa. \tag{70}
$$

Substitution of Eq. (70) into Eq. (69) and re-arrangement yields

$$
\begin{aligned}
&\frac{f(\mathbf{x}_{i+1/2,j},t)-\bar{q}[\mathbf{x}_{i+1/2,j},t]}{\tau}+\left[\frac{\partial\bar{q}}{\partial t}\right]^n_{i+1/2,j}(1-\mathrm{e}^{-\kappa})\\
&\quad=\frac{1}{\tau}\left\{H(c_x)q^n_{i+1/2^-,j}+[1-H(c_x)]q^n_{i+1/2^+,j}-\bar{q}^n_{i+1/2,j}\right\}\mathrm{e}^{-\kappa}\\
&\qquad-\left\{H(c_x)(\nabla q)^n_{i+1/2^-,j}+[1-H(c_x)](\nabla q)^n_{i+1/2^+,j}\right\}\\
&\qquad\bullet\,\mathbf{c}\kappa\mathrm{e}^{-\kappa}+\left[\frac{\partial\bar{q}}{\partial y}\right]^n_{i+1/2,j}c_y[\kappa\mathrm{e}^{-\kappa}-(1-\mathrm{e}^{-\kappa})]\\
&\qquad+\left\{H(c_x)\left[\frac{\partial\bar{q}}{\partial x}\right]^n_{i+1/2^-,j}+[1-H(c_x)]\left[\frac{\partial\bar{q}}{\partial x}\right]^n_{i+1/2^+,j}\right\}\\
&\qquad\times c_x[\kappa\mathrm{e}^{-\kappa}-(1-\mathrm{e}^{-\kappa})].
\end{aligned}
\tag{71}
$$

This equation may be integrated over the particle velocities $\mathbf{c}$ from $-\infty$ to ∞ to obtain

$$
\begin{aligned}
&\int_{-\infty}^{\infty}\int_{-\infty}^{\infty}\frac{f(\mathbf{x}_{i+1/2,j},t)-\bar{q}[\mathbf{x}_{i+1/2,j},t]}{\tau}\,\mathrm{d}c_x\,\mathrm{d}c_y\\
&\quad+\left[\frac{\partial\bar{C}}{\partial t}\right]^n_{i+1/2,j}(1-\mathrm{e}^{-\kappa})\\
&\quad=-\left\{\frac{\partial}{\partial x}\left[\frac{C\bar{u}}{2}\mathrm{erfc}(-\sqrt{\lambda}u)+\frac{1}{2}\frac{\mathrm{e}^{-\lambda u^2}}{\sqrt{\pi\lambda}}\right]^n_{i+1/2^-,j}\right.\\
&\qquad\left.+\frac{\partial}{\partial x}\left[\frac{C\bar{u}}{2}\mathrm{erfc}(\sqrt{\lambda}u)-\frac{1}{2}\frac{\mathrm{e}^{-\lambda u^2}}{\sqrt{\pi\lambda}}\right]^n_{i+1/2^+,j}\right\}\kappa\mathrm{e}^{-\kappa}\\
&\qquad+\left\{\frac{\partial}{\partial x}\left[\frac{\bar{C}\bar{u}}{2}\mathrm{erfc}(-\sqrt{\bar{\lambda}}\bar{u})+\frac{1}{2}\frac{\mathrm{e}^{-\bar{\lambda}\bar{u}^2}}{\sqrt{\pi\bar{\lambda}}}\right]^n_{i+1/2^-,j}\right.\\
&\qquad\left.+\frac{\partial}{\partial x}\left[\frac{\bar{C}\bar{u}}{2}\mathrm{erfc}(\sqrt{\bar{\lambda}}\bar{u})-\frac{1}{2}\frac{\mathrm{e}^{-\bar{\lambda}\bar{u}^2}}{\sqrt{\pi\bar{\lambda}}}\right]^n_{i+1/2^+,j}\right\}\kappa\mathrm{e}^{-\kappa}\\
&\qquad-\left\{\frac{\partial}{\partial x}\left[\frac{\bar{C}\bar{u}}{2}\mathrm{erfc}(-\sqrt{\bar{\lambda}}\bar{u})+\frac{1}{2}\frac{\mathrm{e}^{-\bar{\lambda}\bar{u}^2}}{\sqrt{\pi\bar{\lambda}}}\right]^n_{i+1/2^-,j}\right.\\
&\qquad\left.+\frac{\partial}{\partial x}\left[\frac{\bar{C}\bar{u}}{2}\mathrm{erfc}(\sqrt{\bar{\lambda}}\bar{u})-\frac{1}{2}\frac{\mathrm{e}^{-\bar{\lambda}\bar{u}^2}}{\sqrt{\pi\bar{\lambda}}}\right]^n_{i+1/2^+,j}\right\}(1-\mathrm{e}^{-\kappa})\\
&\qquad-\left[\frac{\partial\bar{C}\bar{v}}{\partial y}\right]^n_{i+1/2^-,j}\kappa\mathrm{e}^{-\kappa}+\left[\frac{\partial\bar{C}\bar{v}}{\partial y}\right]^n_{i+1/2,j}[\kappa\mathrm{e}^{-\kappa}-(1-\mathrm{e}^{-\kappa})].
\end{aligned}
\tag{72}
$$

In this equation, the overbarred quantities are continuous values at the cell boundaries. Designate the first and second terms in braces in Eq. (72) using a shorthand such that

$$\left[\frac{\partial(Cu)}{\partial x}\right]^n_{i+1/2,j} \frac{\partial}{\partial x}\left[\frac{Cu}{2}\mathrm{erfc}(-\sqrt{\lambda}u)+\frac{1}{2}\frac{\mathrm{e}^{-\lambda u^2}}{\sqrt{\pi\lambda}}\right]^n_{i+1/2^-,j} + \frac{\partial}{\partial x}\left[\frac{Cu}{2}\mathrm{erfc}(\sqrt{\lambda}u)-\frac{1}{2}\frac{\mathrm{e}^{-\lambda u^2}}{\sqrt{\pi\lambda}}\right]^n_{i+1/2^+,j}, \tag{73}$$

$$\left[\frac{\partial(\bar{C}\bar{u})}{\partial x}\right]^n_{i+1/2,j} = \frac{\partial}{\partial x}\left[\frac{\bar{C}\bar{u}}{2}\mathrm{erfc}(-\sqrt{\bar{\lambda}}\bar{u})+\frac{1}{2}\frac{\mathrm{e}^{-\bar{\lambda}\bar{u}^2}}{\sqrt{\pi\bar{\lambda}}}\right]^n_{i+1/2^-,j} + \frac{\partial}{\partial x}\left[\frac{\bar{C}\bar{u}}{2}\mathrm{erfc}(\sqrt{\bar{\lambda}}\bar{u})-\frac{1}{2}\frac{\mathrm{e}^{-\bar{\lambda}\bar{u}^2}}{\sqrt{\pi\bar{\lambda}}}\right]^n_{i+1/2^+,j}. \tag{74}$$

Then Eq. (72) may be rearranged to

$$\int_{-\infty}^{\infty}\int_{-\infty}^{\infty}\frac{f(\mathbf{x}_{i+1/2,j},t)-\bar{q}[\mathbf{x}_{i+1/2,j},t]}{\tau}\mathrm{d}c_x\,\mathrm{d}c_y = -\left\{\left[\frac{\partial\bar{C}}{\partial t}\right]^n_{i+1/2,j}+\left[\frac{\partial(\bar{C}\bar{u})}{\partial x}\right]^n_{i+1/2,j}+\left[\frac{\partial\bar{C}\bar{v}}{\partial y}\right]^n_{i+1/2,j}\right\} \times(1-\mathrm{e}^{-\kappa})-\left\{\left[\frac{\partial(Cu)}{\partial x}\right]^n_{i+1/2,j}-\left[\frac{\partial(\bar{C}\bar{u})}{\partial x}\right]^n_{i+1/2,j}\right\}\kappa\mathrm{e}^{-\kappa}. \tag{75}$$

Note that by compatibility condition (20), the left-hand side of this equation should equal zero. This would be the case if both collections of terms in braces were zero. Certainly, the first braced group could be forced to be zero by selecting the time derivative to be equal to the negative of the divergence term. However, the quantities in the second brace have already been determined and the two derivatives will be equal only if the concentration and velocity functions are at least C^1 continuous in the direction normal to the boundary of the cell. For this case, the compatibility condition is satisfied if the time derivative is selected such that

$$\left\{\left[\frac{\partial\bar{C}}{\partial t}\right]+\left[\frac{\partial\bar{C}\bar{u}}{\partial x}\right]+\left[\frac{\partial\bar{C}\bar{v}}{\partial y}\right]\right\}^n_{i+1/2,j}=0. \tag{76}$$

In this instance, the time derivative of $\bar{C}$ at the cell boundary and time t^n may be calculated directly from the spatial derivatives that have previously been calculated. When the last term on the right-hand side of Eq. (75) is not exactly zero, the compatibility condition cannot be satisfied at every instant of time. However, it may be satisfied in an average sense over a time-step by integrating Eq. (75) over that time-step and requiring that the compatibility integral be zero. Since $\kappa=(t-t^n)/\tau$, the integration from t^n to $t^n+\Delta t$ with the requirement that the compatibility condition be satisfied on average over this time interval yields

$$0 = -\left\{\left[\frac{\partial\bar{C}}{\partial t}\right]^n_{i+1/2,j}+\left[\frac{\partial(\bar{C}\bar{u})}{\partial x}\right]^n_{i+1/2,j}+\left[\frac{\partial\bar{C}\bar{v}}{\partial y}\right]^n_{i+1/2,j}\right\} \times\left[\Delta t-\tau(1-\mathrm{e}^{-\Delta t/\tau})\right] + \left\{\left[\frac{\partial(Cu)}{\partial t}\right]^n_{i+1/2,j}-\left[\frac{\partial(\bar{C}\bar{u})}{\partial x}\right]^n_{i+1/2,j}\right\} \times\left[\Delta t\mathrm{e}^{-\Delta t/\tau}-\tau(1-\mathrm{e}^{-\Delta t/\tau})\right]. \tag{77}$$

Thus, the time derivative is determined in terms of the indicated known spatial derivatives. If the time-step is much greater than the collision time (as will typically be the case), then $\Delta t\gg\tau$ and Eq. (76) is recovered. However, here the complete form given by Eq. (77) is employed to determine the time derivative of $\bar{C}$ from the known spatial derivatives. This ensures that the compatibility condition on mass is satisfied, on the average such that the computational scheme will be mass conservative.

Analogous calculations to those in this appendix must be performed to calculate the derivatives in time and space at $\mathbf{x}_{i-1/2,j}$, $\mathbf{x}_{i,j+1/2}$, and $\mathbf{x}_{i,j-1/2}$.

Appendix D. Moments of the Gaussian distribution

The Gaussian distribution for the two-dimensional case is given in Eq. (16) as

$$q(\mathbf{x},\mathbf{c},t)=C\frac{\lambda}{\pi}\exp[-\lambda\mid\mathbf{c}-\mathbf{v}\mid^2] \tag{78}$$

Of interest are the integrals of this distribution over the particle velocities, $\mathbf{c}$, from $-\infty$ to ∞ as well as from 0 to ∞ and from $-\infty$ to 0. In the present study, the following relations have been used:

$$1=\frac{1}{C}\int_{-\infty}^{\infty}\int_{-\infty}^{\infty}q\,\mathrm{d}c_x\,\mathrm{d}c_y, \tag{79}$$

$$\mathbf{v}=\frac{1}{C}\int_{-\infty}^{\infty}\int_{-\infty}^{\infty}\mathbf{c}q\,\mathrm{d}c_x\,\mathrm{d}c_y, \tag{80}$$

$$\mathbf{vv}+\frac{1}{2\lambda}\mathbf{I}=\frac{1}{C}\int_{-\infty}^{\infty}\int_{-\infty}^{\infty}\mathbf{cc}q\,\mathrm{d}c_x\,\mathrm{d}c_y, \tag{81}$$

$$\frac{1}{2}\mathrm{erfc}(-\sqrt{\lambda}u)=\frac{1}{C}\int_{-\infty}^{\infty}\int_{0}^{\infty}q\,\mathrm{d}c_x\,\mathrm{d}c_y, \tag{82}$$

$$\frac{1}{2}\mathrm{erfc}(\sqrt{\lambda}u)=\frac{1}{C}\int_{-\infty}^{\infty}\int_{-\infty}^{0}q\,\mathrm{d}c_x\,\mathrm{d}c_y, \tag{83}$$

$$\frac{u}{2}\mathrm{erfc}(-\sqrt{\lambda}u)+\frac{1}{2}\frac{\mathrm{e}^{-\lambda u^2}}{\sqrt{\pi\lambda}}=\frac{1}{C}\int_{-\infty}^{\infty}\int_{0}^{\infty}c_xq\,\mathrm{d}c_x\,\mathrm{d}c_y, \tag{84}$$

$$\frac{u}{2}\mathrm{erfc}(\sqrt{\lambda}u)-\frac{1}{2}\frac{\mathrm{e}^{-\lambda u^2}}{\sqrt{\pi\lambda}}=\frac{1}{C}\int_{-\infty}^{\infty}\int_{-\infty}^{0}c_xq\,\mathrm{d}c_x\,\mathrm{d}c_y, \tag{85}$$

$$\frac{1}{2}\mathrm{erfc}(-\sqrt{\lambda}v) = \frac{1}{C}\int_0^\infty \int_{-\infty}^\infty q\,\mathrm{d}c_x\,\mathrm{d}c_y, \tag{86}$$

$$\frac{1}{2}\mathrm{erfc}(\sqrt{\lambda}v) = \frac{1}{C}\int_{-\infty}^0 \int_{-\infty}^\infty q\,\mathrm{d}c_x\,\mathrm{d}c_y, \tag{87}$$

$$\frac{v}{2}\mathrm{erfc}(-\sqrt{\lambda}v) + \frac{1}{2}\frac{\mathrm{e}^{-\lambda v^2}}{\sqrt{\pi v}} = \frac{1}{C}\int_0^\infty \int_{-\infty}^\infty c_y q\,\mathrm{d}c_x\,\mathrm{d}c_y, \tag{88}$$

$$\frac{v}{2}\mathrm{erfc}(\sqrt{\lambda}v) - \frac{1}{2}\frac{\mathrm{e}^{-\lambda v^2}}{\sqrt{\pi\lambda}} = \frac{1}{C}\int_{-\infty}^0 \int_{-\infty}^\infty c_y q\,\mathrm{d}c_x\,\mathrm{d}c_y. \tag{89}$$

References

[1] Chen S, Doolen G. Lattice boltzmann method for fluid flows. Ann Rev Fluid Mech 1998;30:329–64.

[2] Chen H, Chen S, Matthaeus WH. Recovery of the Navier–Stokes equations using a lattice-gas Boltzmann method. Phys Rev A 1992;45:R5339–42.

[3] Chu CK. Kinetic-theory description of the formation of shock-waves. Phys Fluids 1965;8:12–21.

[4] Deng J, Ghidaoui MS. Computation of open channel flow using a gas-kinetic based scheme. In: Proceedings of 1998 International Water Resources Engineering Conference. ASCE. 3–7 August; Memphis, Tennessee, USA. 1998;2:1864–1869.

[5] Engquist B, Osher S. Stable and entropy satisfying approximations for transonic flow calculations. Math Comput 1980;34: 45–75.

[6] Frisch U, Hasslacher B, Pomeau Y. Lattice gas for the Navier–Stokes equations. Phys Rev Lett 1986;14:1505–8.

[7] Ghidaoui MS, Deng JQ, Xu K, Gray WG. A Boltzmann-based model for open channel flows. Int J Numer Meth Fluids [in press].

[8] Gunstensen AK, Rothman DH, Zaleski S, Zanetti G. Lattice Boltzmann model of immiscible fluids. Phys Rev A 1991;43(8): 4320–7.

[9] He X, Shen X, Doolen GD. Discrete Boltzmann equation model for non-ideal gases. Phys Rev 1998;57(1):R13–6.

[10] Hirsch C. Numerical computation of internal and external flows: computational methods for inviscid and viscous flows. London: Wiley; 1990.

[11] Inamuro T, Yoshino M, Ogino F. Lattice boltzmann simulation of flows in a three-dimensional porous structure. Int J Numer Meth Fluids 1999;29:737–48.

[12] Jou D, Casas-Vazquez J, Lebon G. Extended irreversible thermodynamics. Berlin: Springer; 1996.

[13] Kim C, Xu K, Martinelli L, Jameson A. Analysis and implementation of the gas-kinetic BGK scheme for computational gas dynamics. Int J Numer Meth Fluids 1997;25:21–49.

[14] Kumar R, Nivarathi SS, Davis HT, Kroll DM, Maier RS. Application of the Lattice–Boltzmann method to study flow and dispersion in channels with and without expansion and contraction geometry. Int J Numer Meth Fluids 1999;31:801–19.

[15] Leonard BP. The ultimate conservative difference scheme applied to unsteady one-dimensional advection. Comput Meth Appl Mech Eng 1991;88:17–74.

[16] LeVeque RJ. Numerical methods for conservation laws. Boston: Springer; 1992.

[17] Martinez DO, Chen S, Matthaeus WH. Lattice Boltzmann magnetohydrodynamics. Phys Plasmas 1994;1:1850–67.

[18] Osher S. Shock modeling in aeronautics. In: Numerical methods for fluid dynamics KWM, Baines MJ. editor. London: Academic Press; 1982. p. 179–218.

[19] Qian YH. Simulating thermohydrodynamics with lattice BGK models. J Sci Comp 1993;8:231–41.

[20] Reitz RD. One-dimensional compressible gas dynamics calculations using the Boltzmann equations. J Comput Phys 1981;42:108–23.

[21] Roe PL. The use of Riemann problem in finite difference scheme. Lecture Notes in Physics 141. Berlin: Springer; 1981a. p. 354–9.

[22] Roe PL. Approximate riemann solvers parameter vectors and difference schemes. J Comput Phys 1981b;43:357–72.

[23] Rothman DH. Cellular-automaton fluids a model for flow in porous media. Geophys 1988;53:509–18.

[24] Rothmann DH, Zaleskim S. Lattice-gas cellular automata simple models of complex hydrodynamics. Cambridge, UK: Cambridge University Press; 1997.

[25] Steger JL, Warming RF. Flux vector splitting of the inviscid gas-dynamic equations with application to finite difference methods. J Comput Phys 1981;40:263–93.

[26] Su M, Xu K, Ghidaoui MS. Low speed flow simulation by the Gas-kinetic scheme. J Comput Phys 1998;150:17–39.

[27] Van Leer B. Towards ultimate conservative difference scheme V: a second-order sequel to Godunov's method. J Comput Phys 1977;32:276–99.

[28] Van Leer, B. (1982). Flux vector splitting for the Euler equations. In: Proceedings of the Eighth International Conference on Numerical Methods in Fluid Dynamics. Berlin: Springer.

[29] Vincenti GH, Kruger CH Jr. Introduction to physical gas dynamics. Malabar, FL, USA: Krieger Publishing; 1965.

[30] Xu K. BGK-based scheme for multicomponent flow calculations. J Comput Phys 1997a;134:122–33.

[31] Xu K. A gas-kinetic scheme for the Euler equations with heat transfer. In: Proceedings of the International Symposium on Computational Fluid Dynamics. Beijing; 1997b. p. 247–52.

[32] Xu K, Kim C, Martinelli L, Jameson A. BGK-based schemes for the simulation of compressible flow. IJCFD 1996;7:213–35.

[33] Xu K, Martinelli L, Jameson A. Gas-kinetic finite volume methods, flux–vector splitting and artificial diffusion. J Comput Phys 1995;120:48–65.

[34] Quirk JJ. A contribution to the great Riemann Solver debate. Int J Numer Meth Fluids 1994;18:555–74.

[35] Hirsch HT. Numerical computation of internal and external flows, vol. 1: fundamentals of numerical discretization. New York: Wiley; 1989.